REPORT DOCUMENTATION PAGE

Form Approved
OMB No. 0704-0188

1. REPORT DATE *(DD-MM-YYYY)*	2. REPORT TYPE	3. DATES COVERED *(From - To)*
31-03-2011	Final Performance Report	15-06-2009 to 31-12-2010

4. TITLE AND SUBTITLE
Experimental Studies of Coal and Biomass Fuel Synthesis and and Flame Characterization for Aircraft Engines (Year Two)

5a. CONTRACT NUMBER

5b. GRANT NUMBER
FA9550-09-1-0494

5c. PROGRAM ELEMENT NUMBER

6. AUTHOR(S)
R. K. Agrawal, J. P. Gore, F. H. Ribeiro, W. N. Delgass, R. Lucht, L. Qiao, S. Naik, A. Smeltz, D. Guildenbecher

5d. PROJECT NUMBER

5e. TASK NUMBER

5f. WORK UNIT NUMBER

7. PERFORMING ORGANIZATION NAME(S) AND ADDRESS(ES) AND ADDRESS(ES)

Purdue University
Energy Center
Mann Hall, Room 266
203 Martin Jischke Drive
West Lafayette, IN 47907-2022

8. PERFORMING ORGANIZATION REPORT NUMBER

9. SPONSORING / MONITORING AGENCY NAME(S) AND ADDRESS(ES)
Air Force Office of Scientific Research
875 North Randolph St.
Suite 325, Room 3112
Arlington, VA 22203-1768

10. SPONSOR/MONITOR'S ACRONYM(S)

11. SPONSOR/MONITOR'S REPORT NUMBER(S)

12. DISTRIBUTION / AVAILABILITY STATEMENT
Approved for public release; distribution is unlimited

13. SUPPLEMENTARY NOTES

14. ABSTRACT
Several prototype, fast-pyrolysis reactors were built and tested to explore various reactor configurations. A high-pressure, fast-hydropyrolysis reactor system was designed based on the prototype, cyclone-type, fast-pyrolysis reactor. In addition, experiments were completed using a micro-scale reactor to better understand the fundamentals of char formation during fast-pyrolysis and fast-hydropyrolysis. To study coal gasification in the presence of excess hydrogen, an optically accessible, high-pressure and high-temperature entrained flow gasifier was constructed. This system utilizes a novel H_2-O_2 chemical steam generator to produce super-critical steam, and, when the steam generator is operated with equivalence ratios greater than one, gasification in a H_2 rich environment can be studied. Tunable diode laser based in-situ gas species concentration measurements and detailed chemistry computations of the gasification process have been initiated. Finally, to analyze the combustion performance of the proposed synthetic liquid fuels, an opposed flow burner was constructed. Particle image velocimetry was used to quantify the velocity flow fields at various operating conditions. The results will be useful for simulation of counter-flow flames using axi-symmetric 2-D flame codes.

15. SUBJECT TERMS
Biomass fast hydropyrolysis, hydrodeoxygenation, and coal steam pyrolysis, diode laser flame structure studies, computational flame structure studies

16. SECURITY CLASSIFICATION OF: Unclassified			17. LIMITATION OF ABSTRACT	18. NUMBER OF PAGES	19a. NAME OF RESPONSIBLE PERSON
a. REPORT	b. ABSTRACT	c. THIS PAGE	UL	58	Julian Tishkoff
Unclassified	Unclassified	Unclassified			19b. TELEPHONE NUMBER *(include area code)* (703)696-8478

Experimental Studies of Coal and Biomass Fuel Synthesis and Flame Characterization for Aircraft Engines

AFOSR Grant Number: FA9550-09-1-0494

Final Performance Report

Report Period: June 15, 2009 to December 31, 2010

Prepared by:

Dr. Rakesh Agrawal (PI)
765-494-4811
765-494-0805 (fax)
agrawalr@purdue.edu

Dr. Jay Gore (Co-PI)
765-494-1610
765-496-9322 (fax)
gore@purdue.edu

Dr. Fabio H. Ribeiro (Participating Investigator)
Dr. W. Nicholas Delgass (Participating Investigator)
Dr. Robert P. Lucht (Participating Investigator)
Dr. Li Qiao (Participating Investigator)
Dr. Sameer Naik
Dr. Andrew Smeltz
Dr. Daniel Guildenbecher

School of Chemical Engineering
School of Mechanical Engineering
School of Aeronautics and Astronautics

Purdue University
West Lafayette, IN 47907

Table of Contents

Executive Summary

AFOSR Grant Number: FA9550-09-1-0494
Project Title:
Experimental Studies of Coal and Biomass Fuel Synthesis and Flame Characterization for Aircraft Engines (Year Two)
Project Period: June 15, 2009 to December 31, 2010
Report Period: June 15, 2009 to December 31, 2010
Date of Report: March 31, 2011
Contacts:
Rakesh Agrawal Phone: 765-494-4811, E-mail: agrawalr@purdue.edu
Jay Gore, Phone: 765-494-1610, E-mail: gore@purdue.edu

Project Objective:
The broad objective of the research team is to establish the feasibility of an innovative idea to develop a commercially and technically viable integrated coal/biomass-to-liquid jet fuel synthesis process while mitigating the CO_2 penalty. The production of transportation fuel from domestic coal and biomass sources would assure the U.S. Air Force a dependable and secure fuel supply. However, low efficiencies of the existing coal/biomass-to-liquid fuel processes, high capital and operating costs of the coal gasifiers and lack of combustion characteristics of the liquid fuel from coal/biomass are some of the major barriers to their use. As a result, there is a need for fundamental scientific and synergistic research in catalytic biomass fast-hydropyrolysis, advanced coal gasification and liquid fuel combustion studies. The objective of this project was to develop experimental facilities for addressing specific scientific issues associated with the utilization of biomass and coal to produce appropriate aviation liquid fuels.

Several prototype, fast-pyrolysis reactors were built and tested to explore various reactor configurations. A high-pressure, fast-hydropyrolysis reactor system was designed based on the prototype, cyclone-type, fast-pyrolysis reactor. Construction of the reactor is nearly finished. In addition, experiments were completed using a micro-scale reactor to better understand the fundamentals of char formation during fast-pyrolysis and fast-hydropyrolysis. To study advanced gasification, a high-pressure and high-temperature entrained flow gasifier was constructed. This system utilizes a novel H_2-O_2 chemical steam generator to produce super-critical steam, and, when the steam generator is operated with equivalence ratios greater than one, gasification in a H_2 rich environment can be studied. The entrained flow gasifier is fully operational and will be utilized to study advanced gasification mechanisms. Finally, to analyze the combustion performance of the proposed synthetic liquid fuels, an opposed flow burner was constructed. Particle image velocimetry was used to quantify the velocity flow fields at various operating conditions. The results will be useful for simulation of counter-flow flames using axi-symmetric 2-D flame codes. In summary, this project has successfully developed unique experimental facilities for study of the coal/biomass-to-liquid fuel synthesis process. The experimental findings will improve the scientific knowledge of catalytic biomass fast-hydropyrolysis, coal/biomass gasification and liquid fuel combustion.

AFOSR grant funds and voluntary cost share funds for the second year of the project have been fully (100%) expended.

1.0 Biomass Fast Hydropyrolysis

Utilization of biomass to supplement liquid aviation fuels from traditional, non-renewable resources requires the conversion of biomass, a rich source of partially-oxidized hydrocarbons, into liquids that are stable and have energy densities and combustion properties that are comparable to those of traditional liquid fuels. The ultimate goal of the proposed catalytic, fast-hydropyolysis process is to meet these requirements by thermally decomposing biomass into small molecules while simultaneously upgrading these products to high-energy-density liquid fuels using one or more catalysts in the presence of high-pressure hydrogen generated by coal gasification.

Research has been focused on two important aspects of biomass fast-hydropyrolysis: Development of a lab-scale, continuous-flow, fast-hydropyrolysis reactor system and fundamental studies of biomass fast-hydropyrolysis utilizing commercially available, as well as custom, micro-scale, batch reactor equipment. Specifically, the work completed to date has:

(1) Designed, built, and tested several prototype, lab-scale, fast-pyrolysis reactors with varying configurations;
(2) Designed and are currently building a lab-scale, high-pressure, fast-hydropyolysis reactor based on results from prototype reactor experiments; and,
(3) Completed experiments with micro-scale, model reactor systems to better understand the fundamentals of fast-pyrolysis and fast-hydropyrolysis.

Experiments were performed with cellulose particles of 20-50 μm as representative of biomass particles. Cellulose particles were used to simplify the experiments in order to gain an early understanding of the complex reaction chemistry and products. Planned experiments to test water-gas-shift catalysts under fast-hydropyrolysis conditions (Tasks 1.3-1.5) were not completed due to delays in completing Task 1.2.

1.1 Experimental Fast-Pyrolysis Studies at High and Low Pressure: Construction and Testing of Prototype Fast-Pyrolysis Reactor Designs

Bridgwater and Peacock [1.1] have reviewed various fast-pyrolysis reactor types, all of which operate at atmospheric pressure or in partial vacuum. To date, little or no work on high-pressure, fast-pyrolysis reactors has been reported in the literature. Hence, there was a need to develop a high-pressure reactor and a low-flowrate, high-pressure, solids feeder from the ground up. Previously, a working screw feeder that operates at pressures up to 68 bar and flowrates from 0.1-5 g min^{-1} was built in the lab and is shown in Figure 1.1. Here, design and testing of two, prototype, high-pressure reactors are described. The results of this work on the prototype reactors were then used to design and build a high-pressure, fast-hydropyrolysis reactor system, which is described in Section 1.2.

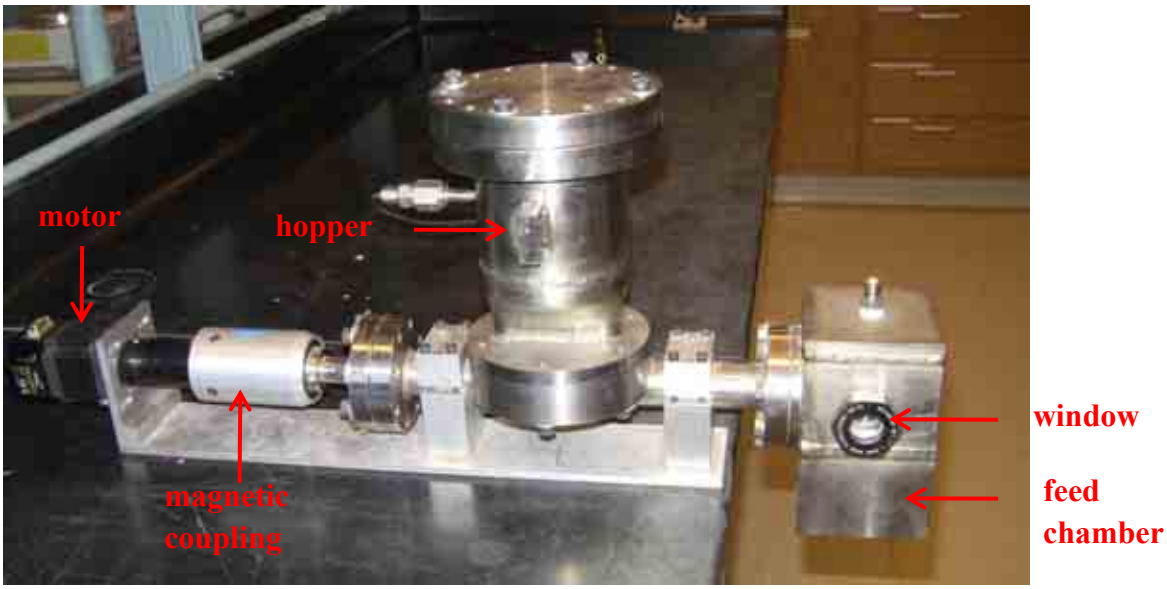

Figure 1.1: Picture of the high-pressure screw feeder

1.1.1 Design, Construction, and Testing of a Free-Fall-type Fast-Pyrolysis Reactor

The most straight-forward pyrolysis reactor configuration found in the literature is the free-fall reactor. Biomass falls through a column of flowing, hot gas inside a vertical, heated vessel which heats the biomass to the desired decomposition temperature by convection and thermal radiation. The residence time of biomass in the reactor is function of reactor height, biomass particle size and density, and gas velocity and density in the reactor and can be calculated from simple particle dynamics [1.2]. Free-fall reactors are typically several meters in height to provide a particle residence time on the order of 1-5 seconds. Inert gas sweeps the products of pyrolysis from the reactor to a series of condensation and gas/liquid separation unit operations. This type of reactor design can be adapted to a high-pressure environment by simply increasing the wall thickness of the reactor to account for the additional stress put on the walls of the reactor from elevated operating pressures. One advantage of operating this type of reactor at high pressure in a hydrogen environment is that the heat transfer rates between the particle and hot gas are significantly improved due to the increase in gas density and thermal conductivity.

In most free-fall reactor designs, both carrier gas and biomass are heated after entering the main body of the reactor. This version requires additional residence time, and therefore height, in order to achieve the desired reaction temperature. Because of a reactor height restriction in the lab, the free-fall reactor design included a hot gas feed which was immediately mixed with incoming biomass. Heat transfer and particle velocity calculations for 50 µm cellulose particles falling through a column of hot He or H_2 gas at 67 bar and 550 °C indicated that a reactor height of about 60 cm, just under the maximum height constraint in the laboratory, was sufficiently tall to heat the biomass to >500 °C. Therefore, the reactor was designed with a pre-heated gas feed. Several reactors with varying inlet configurations were investigated to see if it was possible to have good conversion of biomass to vapors with a 60 cm reactor. The results from these experiments are summarized below.

1.1.1.1 Experimental Methods

Four different free-fall reactor inlet designs, shown in Figure 1.2, were tested using cellulose as a model biomass feedstock. A picture of the reactor setup inside the fume hood is shown in Figure 1.3. The main body of the reactor had an OD of 2.5 cm, ID of 1.9 cm and height of 61 cm. All parts of the reactor were constructed using 316 stainless steel. A coil of tubing inserted inside a ceramic furnace was used to preheat He carrier gas and the reactor was heated using laboratory heating tape.

Condensable products from pyrolysis were collected in two stages. The first stage comprised a concentric tube heat exchanger, cooled with a mixture of ethylene glycol and water, and a Swagelok coalescence filter. The second stage comprised a cold finger trap cooled externally with liquid nitrogen. The flowrate of cellulose was varied between 0.1 to 0.5 g min^{-1}. Nitrogen was used for the screw feeder carrier gas and its flow was varied between 1 to 5 std. L min^{-1}. The flowrate of pre-heated He was varied between 5 to 20 std. L min^{-1}.

Experiments were also performed, using a 5-point thermocouple with temperature measurement locations every 1.25 cm shown in Figure 1.4, to obtain the temperature profile in the first 10-20 cm of the reactor. These data were collected to aid the understanding of the effect of process variables on the temperature distribution within the reactor. This temperature profile information was then correlated with reactor performance.

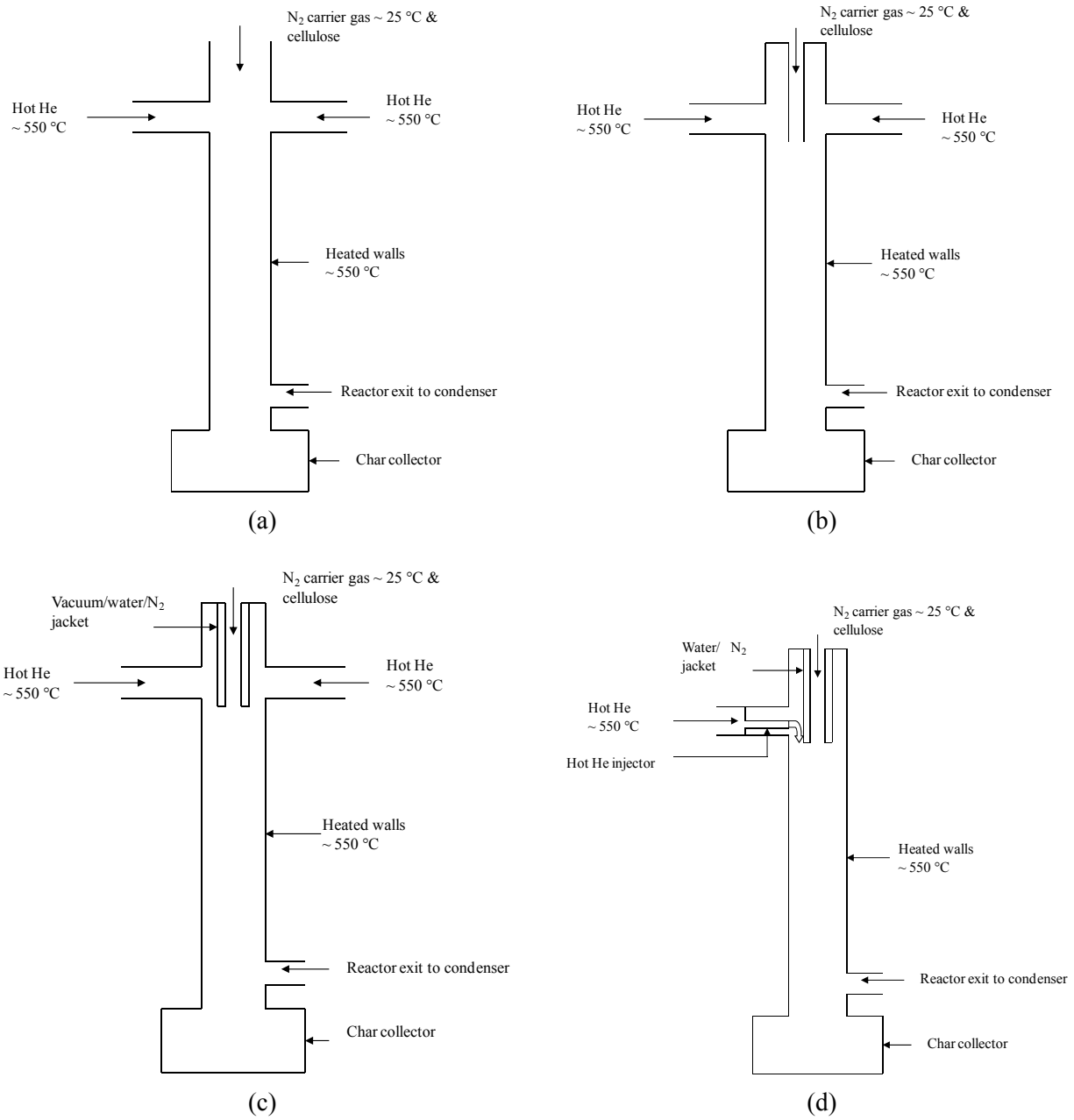

Figure 1.2: Schematics of different designs of the free-fall type fast-pyrolysis reactor that were tested

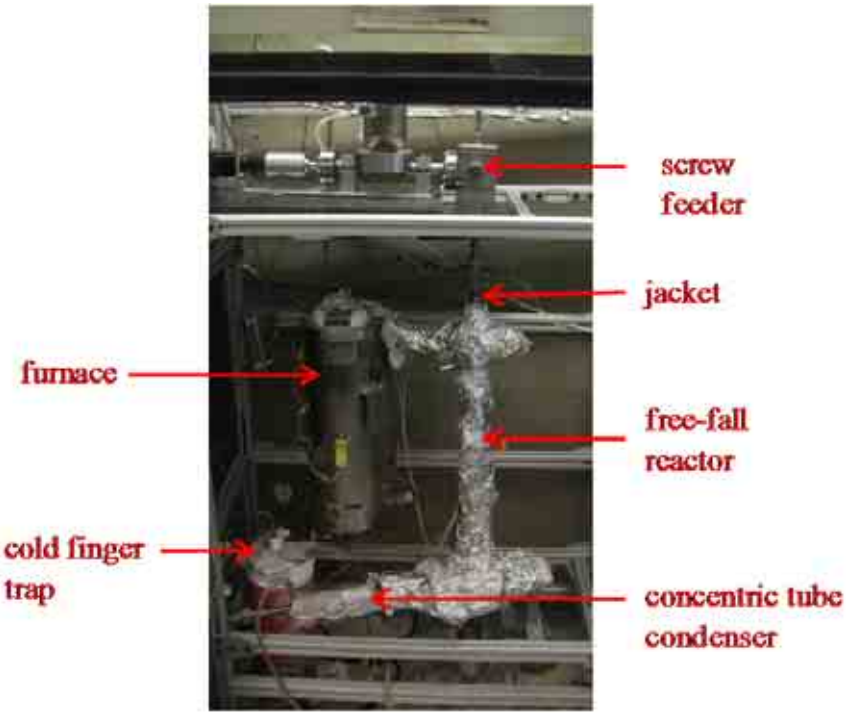

Figure 1.3: Picture of the final design of free-fall type fast-pyrolysis reactor

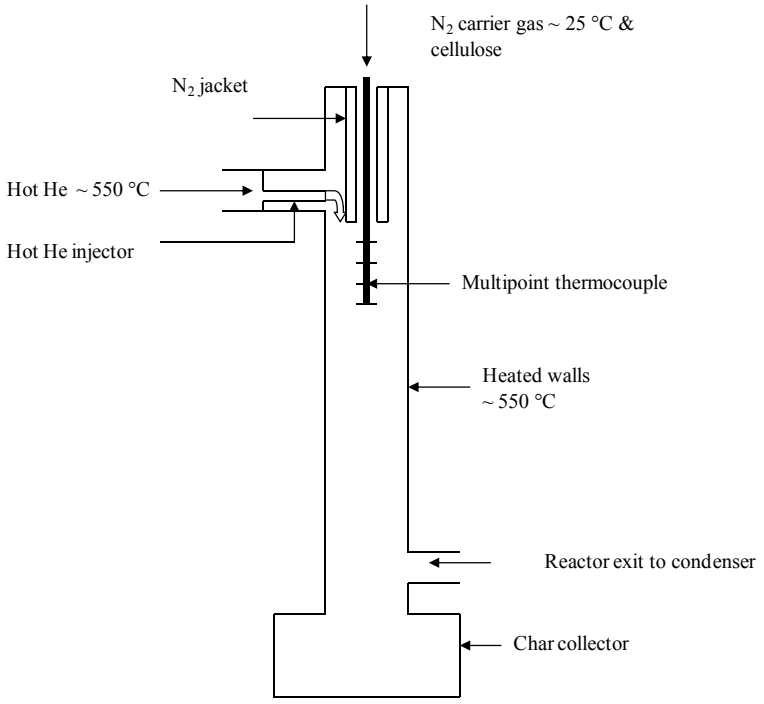

Figure 1.4: Schematic of the final design of the free-fall type fast-pyrolysis reactor with a 5-point thermocouple

1.1.1.2 Results and Discussion

The inlet designs shown in Figure 1.2 were tested in the order shown in the figure, i.e. from the simplest design to the most complex. The inlet design shown in 1.2a consistently clogged due to significant char build up at the mixing junction (cross) where the hot helium mixed with the cellulose. At least two factors led to consistent clogging with this design. First, the gas temperature in this region was high enough to initiate cellulose pyrolysis but not high enough to eliminate significant char formation and subsequent buildup. Previous experiments performed in the lab suggest that gas temperatures in the range of 300-450 °C will lead to significant char formation. Second, disruptive flow patterns caused the cellulose to contact the side walls of the mixing junction where it would stick and form char, eventually leading to a clog. Clogging occurred regardless of cellulose mass flowrate and flowrates of cold and hot gas.

In an attempt to avoid clogging in the mixing junction, a down-tube was added to the inlet, as shown in Figure 1.2b, to try to minimize the rate of heat transfer to the cellulose until after the mixing junction and thus avoid char build up in the mixing junction area. Instead, the cellulose started charring while still inside the small diameter down-tube due to significant heat transfer from the hot helium to the inner wall of the down-tube. The char stuck to the inside wall and formed a clog within minutes of initiating the experiment. Increasing the flowrate of N_2 carrier gas such that the down-tube did not clog resulted in unacceptably low conversion of the cellulose to vapor and permanent gases as well as clogging due to accumulation of char on the walls of the main body of the reactor.

To decrease the rate of heat transfer from the pre-heated He to the inner wall of the down-tube, a metal jacket with a 1-2mm gap between the outer and inner tube was welded to the down-tube, as shown in Figures 1.2c,d. This annular region could be evacuated by a vacuum pump or actively cooled with flowing gas or liquids. Using a vacuum, the ideal insulator, to try and insulate the inner tube was intended to prevent cellulose and the carrier gas from heating without significantly cooling the pre-heated He. Instead, the cellulose charred and clogged at the tip of the down-tube, due to heat conduction where the outer jacket was welded to the inner tube. Using water or nitrogen to actively cool the inner down-tube was successful in preventing clogging in the inlet section of the reactor. However, the reactor simply clogged due to char build up in the main body of the reactor due to significant reduction in gas temperatures inside the main body of the reactor. The addition of a hot-gas injector, shown in Figure 1.2d, to direct pre-heated gas around the down-tube also did not improve reactor reliability.

In experiments where cellulose clogged in the main body of the reactor due to significant char formation on the inside walls, it was observed that the location of the clog varied with the flowrate of pre-heated and carrier gases and the wall temperature. This suggested that there is a temperature range in which char formation is maximized. That is, if the cellulose is exposed to moderate temperatures, ~100-150 °C below the ideal pyrolysis temperature of 500-550 °C, it will "caramelize" and form char instead of vapors and gases. Experiments were carried out in an attempt to optimize the temperature profile within the main body of the reactor, again measured using the 5-point thermocouple shown schematically in Figure 1.4. Ideally, the temperature in the reactor should climb as quickly as possible to >500 °C below the down tube to limit char formation reactions and maximize vapor and gas formation.

Using this approach, the temperature profile was optimized by varying the carrier and pre-heated gas flowrates and the external wall temperature of the reactor. The optimized temperature profile corresponded to the steepest gradient which could be achieved after keeping the cellulose from heating prematurely within the down tube. With this optimized profile, the reactor still clogged near the tip of the down tube.

1.1.1.3 Conclusions

All attempts to get the free-fall reactor to work adequately by exploring a wide variety of conditions and inlet configurations for cellulose as a model biomass feedstock failed. After many attempts to improve time on stream, the reactor was still unable to run for more than a few minutes before it clogged. Additionally, the vapor residence time was high enough in this type of reactor, due to the inherently large reactor volume needed for adequate particle residence time, to allow increased conversion of desirable, primary products into undesirable secondary, low-molecular-weight, permanent gases. This type of reactor has been successfully run at atmospheric pressure at larger scales (higher internal diameter and height) [1.3], which help reduce clogging and eliminate the need for high heating rates near the biomass feed inlet. However, such reactor scales are outside the scope of this project.

1.1.2 Design, Construction, and Testing of a Cyclone-type Fast-Pyrolysis Reactor

After repeated failures with the free-fall reactor, alternative reactor designs were reviewed. Because of space limitations in the laboratory, one type of reactor design that seemed promising was the cyclone reactor, first reported on by Lede *et al.* [1.4, 1.5]. Traditionally, cyclones are used for separation of small, micron to millimeter-sized solid particles from high-velocity gases by centrifugal forces generated by the cyclone geometry. As separation occurs, solids fall to the bottom of the cyclone into a collection vessel while gases flow around a down-tube placed in the center of the cyclone and out the top as shown in Figure 1.5. In a cyclone-type, fast-pyrolysis reactor, the inner walls of the cyclone are heated to 500 °C to 550 °C which, in turn, heats the biomass and carrier gas that is fed to the cyclone to the reaction temperature. Char and unreacted biomass are immediately separated from the pyrolysis vapors within the cyclone and pyrolysis vapors and permanent gases flow out the top to condensing systems where liquids are separated from gases. For the work presented here, the existing, in-house equipment was modified to build a prototype reactor system to test the feasibility of operating this type of reactor. The results of these studies have been used to guide the construction of a new cyclone-type, high-pressure, fast-hydropyrolysis reactor which is discussed in Section 1.2.

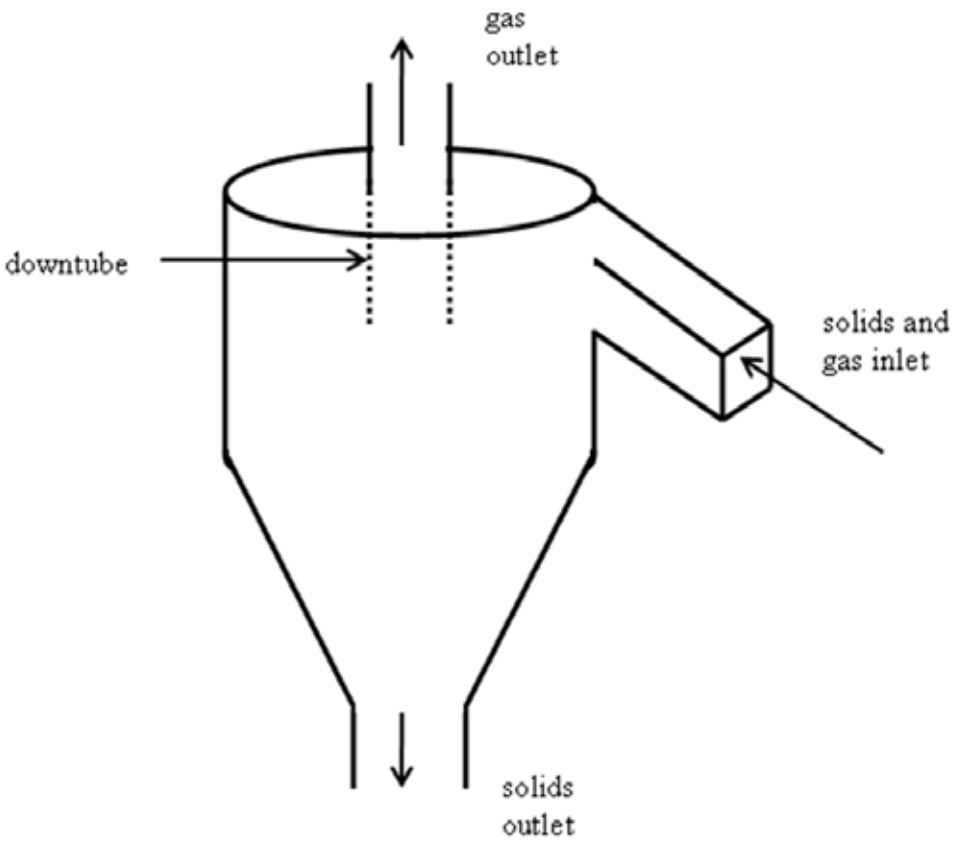

Figure 1.5: Schematic of a conventional cyclone separator used for solid-gas separation

1.1.2.1 Experimental Methods

A schematic of the prototype cyclone reactor and a process flow diagram are shown in Figures 1.6 and 1.7 respectively. Cellulose was fed to the reactor through the high-pressure screw feeder shown in Figure 1.1. Nitrogen was used as a carrier gas through the screw feeder feed chamber and helium was used as the cyclone inlet "sweep gas" for the cellulose. The mixture of cellulose and inert gases was preheated just prior to entering the reactor. The preheating section, reactor, and transfer lines were heated using laboratory heating tape. The inlet gas and cellulose mixture entered tangentially to the wall of the cyclone and were heated to pyrolysis temperature by direct contact with the hot walls. Char and unreacted cellulose were separated from the pyrolysis vapors and collected in the char collector connected to the bottom of the cyclone reactor. Pyrolysis vapors exited the top of the reactor and then passed through a heat-traced transfer line to a two-stage, condenser and gas-liquid separation unit operation to collect liquid products. The first stage was comprised of a concentric-tube heat exchanger, cooled with a circulating mixture of ethylene glycol and water, and a coalescing filter. The second stage was comprised of a cold-finger-type vapor trap (Figure 1.9) cooled externally with liquid N_2 or water/ice mixtures. Permanent gases were then passed through a back-pressure regulator before being exhausted. Due to the absence of gas analysis equipment, gas yields were estimated by subtraction from the overall mass balance.

The cyclone reactor was 2.63" ID and 2.87" OD and made from 316 stainless steel. The total internal volume of the reactor was 0.46 L. The inlet to the reactor was a ¼" OD stainless-steel 316 tube. Bottom and top exits were through ¾" OD welded tubes. The condenser was connected to the reactor through a transfer line comprised of fittings equivalent to a ¾" OD SS316 tube. The tube side of the condenser was made from a ¾" OD SS316 tube and the shell side of 1.5" OD SS316 tube. The total length of the condenser section was 10".

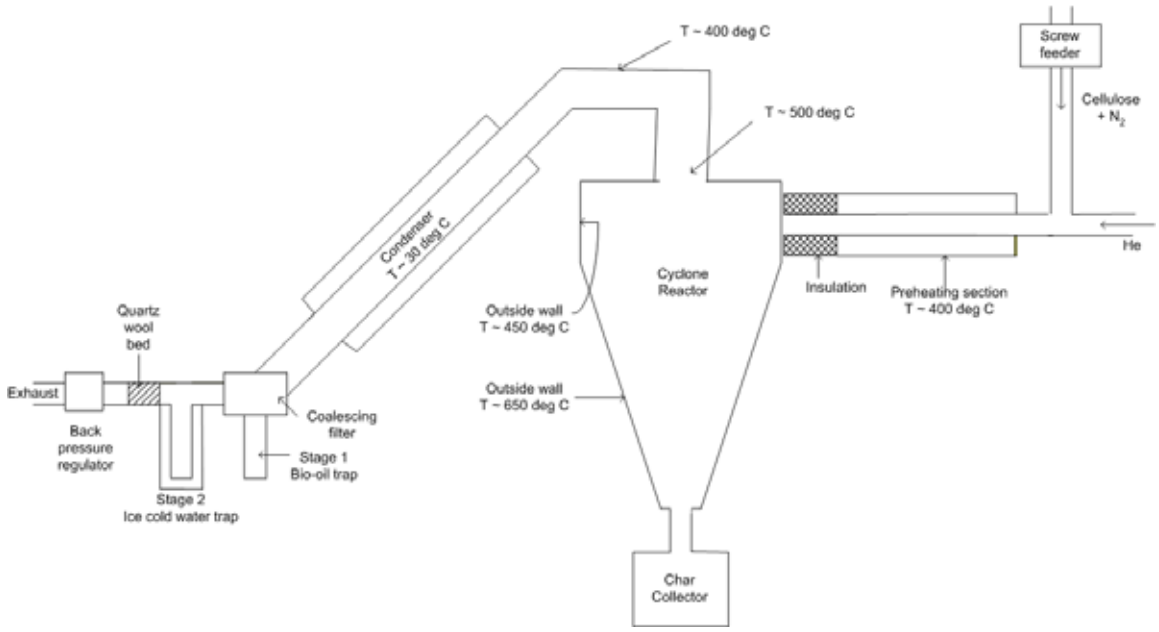

Figure 1.6: Schematic of the cyclone-type fast-pyrolysis reactor

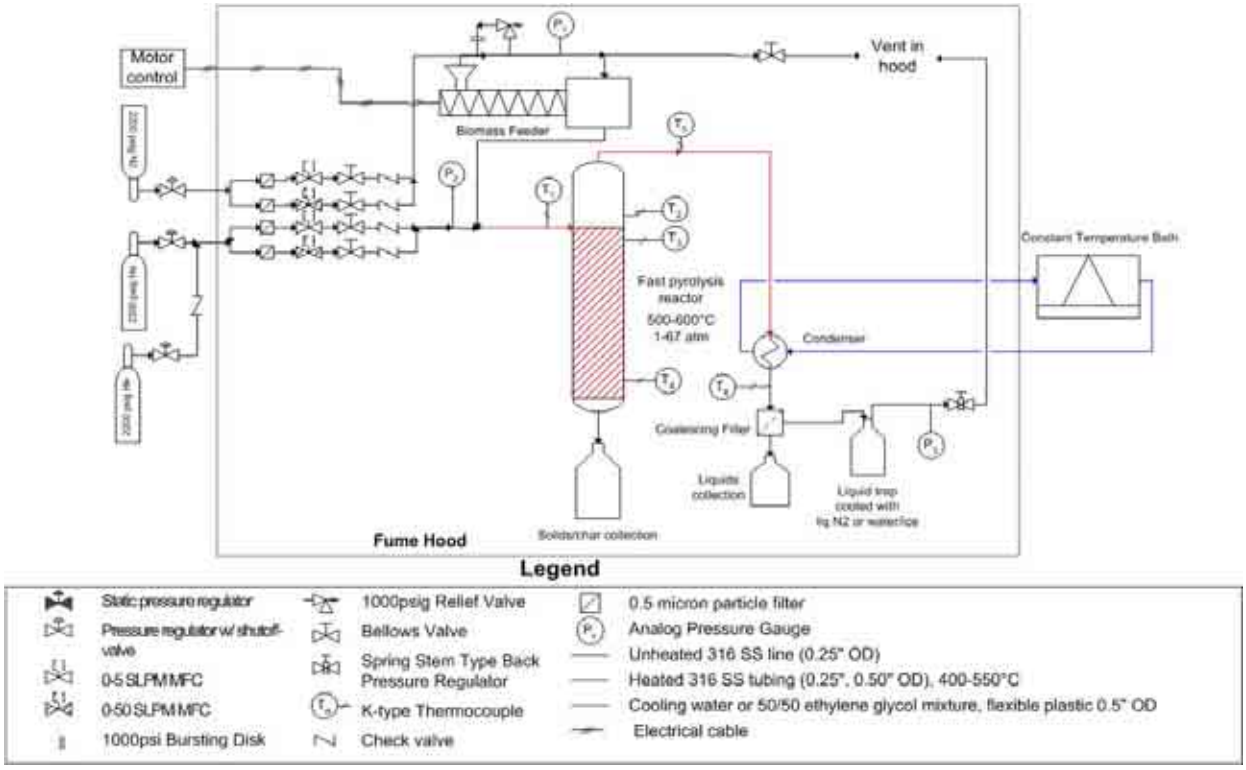

Figure 1.7: Process flow diagram of the cyclone-type fast-pyrolysis reactor

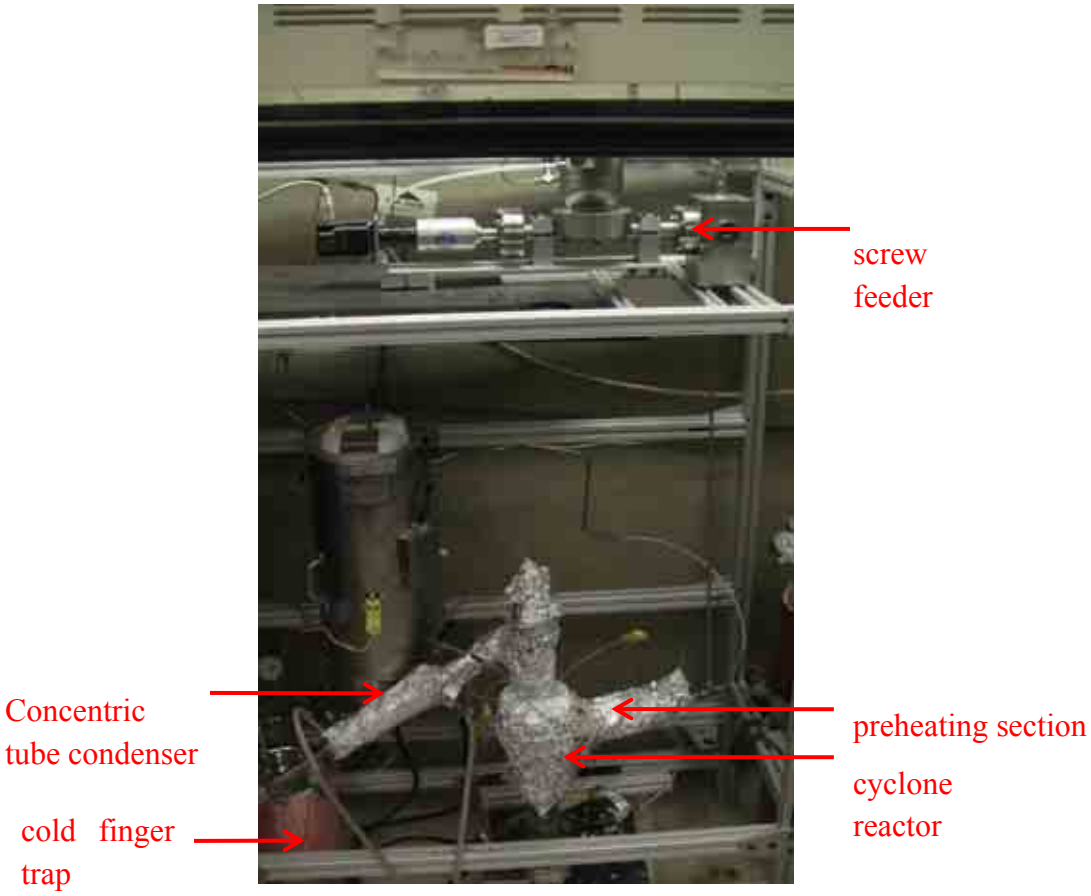

Figure 1.8: Picture of the cyclone-type fast-pyrolysis reactor

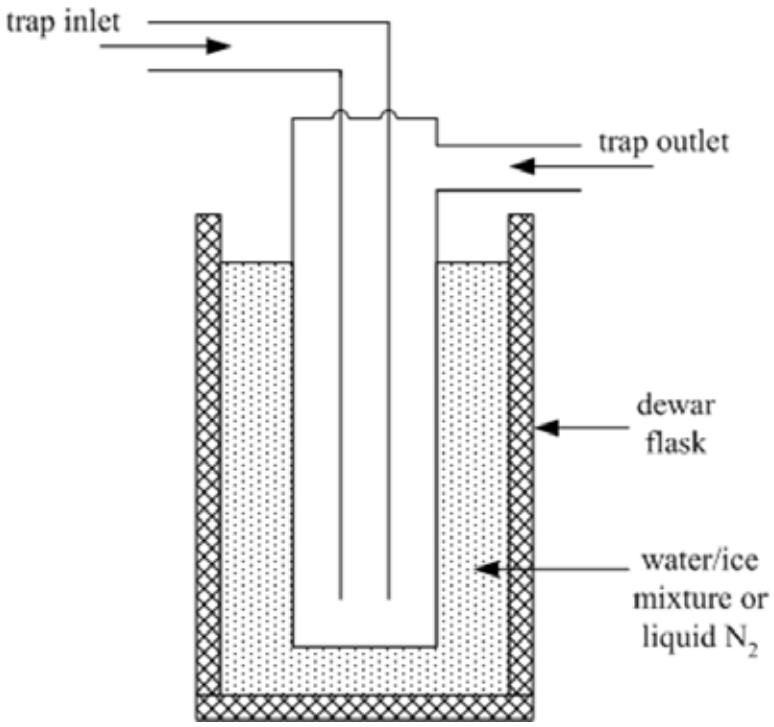

Figure 1.9: Schematic of the cold-finger-type vapor trap

1.1.2.2 Results and Discussion

Initial shake-down experiments failed due to charring and clogging of cellulose at the inlet feed to the cyclone reactor. This problem was resolved by increasing the gas velocity and moderating the temperature in the preheating section, which in turn increased particle entrainment and decreased premature biomass decomposition and, therefore, eliminated settling and char formation in the feed tube. In addition, clogging due to char build up at the mixing junction was eliminated by not preheating the He "sweep gas" before biomass was added to the process stream. Figures 1.7 and 1.8 show the working configuration. All experiments reported here were completed with this pre-heating configuration.

Table 1.1 summarizes the experiments completed on the prototype cyclone reactor after the initial shakedown tests. For experiments #1 and #2, the system pressure was held at 27 bar and the temperature of the transfer line from the reactor to the condenser system was varied to determine the minimum temperature that avoided condensation of pyrolysis vapors while minimizing secondary, homogeneous decomposition reactions of product vapors. In experiments #3-#6, the system pressure was set to 4.5 bar and the total gas flowrate was varied to study the effect of pressure, vapor residence time, and gas velocity on liquid product yield. Experiment #7 was a repeat of experiment #5 with the Stage 1 condenser temperature increased from ~30 °C to ~ 60 °C in an attempt to increase the separation of water from the overall mixture by taking advantage of differences in vapor/liquid equilibrium for water versus the product vapors.

Table 1.1: Summary of the experiments with the cyclone-type fast-pyrolysis reactor using 50 µm microcrystalline cellulose as the biomass model feedstock.

Experiment	#1	#2	#3	#4	#5	#6	#7
Total Mass Fed / g	99.4	29.1	74.8	126.9	28.5	106.2	90.0
Mass Flowrate / g min^{-1}	1.0	1.0	4.4	2.1	1.0	2.4	3.0
Helium Flowrate / (std) L min^{-1}	20.0	20.0	10.0	12.5	15.0	17.5	15.0
Nitrogen Flowrate / (std) L min^{-1}	1.0	1.0	1.0	1.0	1.0	1.0	1.0
Pressure / bar	27.0	27.0	4.5	4.5	4.5	4.5	4.5
Vapor Residence Time in Reactor* / s	14.4	14.4	4.6	3.7	3.1	2.7	3.1
Cyclone Inlet Velocity / cm s^{-1}	156	156	493	606	718	830	718
Transfer Line Temperature / °C	460	429	396	401	400	402	401
Conversion / %	100	99	100	100	99	100	~100
Liquid Yield / %	72	76	37	47	54	65	57
Stage 1 / %	65	71	35	37	43	32	47
Stage 2 / %	7	5	2	10	11	33	10
Char Yield / %	5.1	4.0	1.3	1.2	1.8	1.0	1.1
Gas Yield / % (by balance)	23	20	62	52	44	34	42

*Assuming an average gas temperature of 450 °C and reaction pressure.

At 27 bar, experiments #1 and #2, liquid product yields were 72% and 76% respectively. Figure 1.10 shows the liquids collected in stage 1 and stage 2 condensers from experiment #1. The liquid collected in stage 1 is darker in color and more viscous than that from stage 2. As expected, the two stage condensation and separation system was able to separate some of the water from the overall product mixture. Using liquid nitrogen to cool the stage 2 trap resulted in clogging due to the formation of water-ice in the trap. A mixture of water and ice was used as the coolant in later experiments to avoid this problem. The solids (char) yield in both experiments was 4-5%. The low char yield indicates that this reactor design provides sufficiently high heat transfer rates between the wall of the reactor and the gas/cellulose mixture. Char build up was found on the inner walls of the cyclone opposite to the feed inlet. In the future, this char build up could be minimized by continuously cleaning the wall during the experiment by co-feeding sand (or catalyst) with the biomass. Permanent gas yields of about 23% and 20% were calculated by subtraction from the overall mass balance. Visual inspection of the transfer line indicated that a temperature of about 400ºC on the outside of transfer lines from the reactor to condenser system was adequate to keep the products vaporized.

Figure 1.10: Picture of liquid products from experiment #1. Stage 1 liquid (left) and Stage 2 liquid (right)

Figure 1.11 shows that the liquid yield decreases with vapor residence time at 4.5 bar. It was expected that lower vapor residence times in the reactor would result in a decrease in secondary decomposition reactions of the vapors to gaseous products. Unfortunately, due to a lack of gas phase analysis, this explanation of Figure 1.11 cannot be verified with data to show the expected decrease in permanent gases at higher liquid yield

In experiments #3 to #6, more liquids were collected in Stage 2 as the residence times through the reactor decreased, which suggested that residence time in the Stage 1 of condensing system was not sufficient to cool and condense all of the vapor-phase products. Indeed the outlet temperature of the first condenser was ~50 °C for the low-pressure experiments. Finally, the separation efficiency of the Swagelok coalescence filter decreases with gas velocity which could also explain why more liquids were found in the stage 2 vessel.

In experiment #7, the increase in Stage 1 condenser temperature did appear to increase the separation of water from the organic pyrolysis products by only condensing high boiling point, hydrocarbon-based products of cellulose pyrolysis without any decrease in liquid yield. Residual light organics and the remaining water were collected in the cold-finger trap instead. In future experiments, however, the second stage will only act as a residual liquid trap while the first stage will perform the complete separation.

Interestingly, the average liquid product yield for experiments at 4.5 bar was 52±11%, much lower than that measured at 27 bar, even though the overall vapor residence time was significantly lower at low pressure. One possible explanation is that the increase in gas velocity at low pressure increased the rate of liquid loss into the exhaust stream. After de-construction of the reactor system, significant buildup of tar on the outlet of the separation system, backpressure regulator, and vent lines indicated that there was indeed some bypass of condensable products. In addition, more water was necessarily carried out in the vapor phase at low pressure due to a higher vapor-phase mole fraction. Assuming that the carrier gas is in equilibrium with pure water, the amount of water lost due to differences in operating pressure between the high and low-pressure experiments was calculated. Adding this additional water to the measured liquid yields increased the average liquid yield for the low-pressure experiments to 59±13%. This additional water can explain approximately 50% of the differences in liquid yield between the high and low-pressure

experiments. Again, because of the lack of gas-phase analysis for these experiments, it is not known if gas production actually increased at the expense of liquid products in the low-pressure experiments.

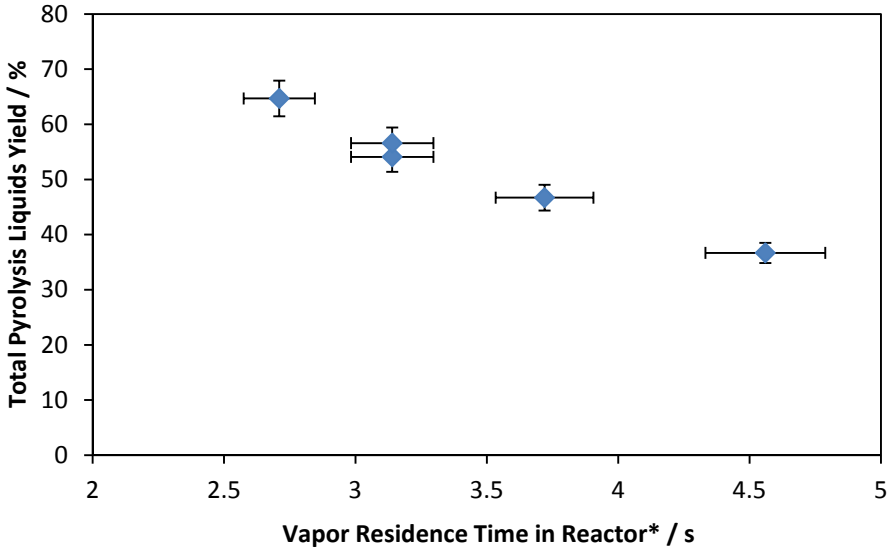

* at pyrolysis temperature = 450 ºC and pyrolysis pressure = 4.5 bar

Figure 1.11: Variation of total pyrolysis liquid yield with vapor residence time for experiments #3 to #7 in the prototype cyclone-type fast-pyrolysis reactor

Qualitatively, the liquid product obtained from the experiments at 4.5 bar was more viscous as compared to the liquid collected at 27 bar. Without quantitative analysis of the oil, it is not possible to know if the molecular weight distribution increased in the low-pressure experiments, however, there is no reason to suggest that it did. In fact, the decrease in char yield suggests that the pyrolysis was more efficient at low pressures, which is discussed further below. The most plausible explanation for the increase in oil viscosity is the decrease in water content, which was calculated above. In other words, less water will condense out at low pressures and therefore the product can be expected to contain less water at low pressure. Additional, more carefully controlled experiments will be needed to decouple the effects of vapor residence time and pressure on fast-pyrolysis of biomass.

Figure 1.12 shows how the amount of char formed during reaction varied with gas velocity in the reactor at 4.5 bar. The decrease in char yield with gas velocity may have been due to increased heat transfer rates between the gas and particles and the wall of the reactor. This hypothesis can also explain why the amount of char increased with total pressure, 1-2% compared to 4-5% at 4.5 and 27 bar, respectively. Residual char was found mainly on the inner wall of the cyclone opposite to the feed inlet tube. The heat transfer from the wall to the carrier gas and biomass particles was likely to have been higher for the low-pressure experiments due to higher gas velocities at the wall. The walls of the reactor were also noticeably cleaner after reaction, possibly due to increased gas velocity that may have helped sweep char away from the walls, which improved heat transfer rates. It is possible that some of the char was entrained with the carrier gas due to high gas velocities and ended up in the oil. This entrained char may also contribute to explaining why the oil was found to be more viscous than in the high-pressure experiments. For future

experiments, the oil will be filtered to determine the amount of char carryover to the liquid collection unit operation.

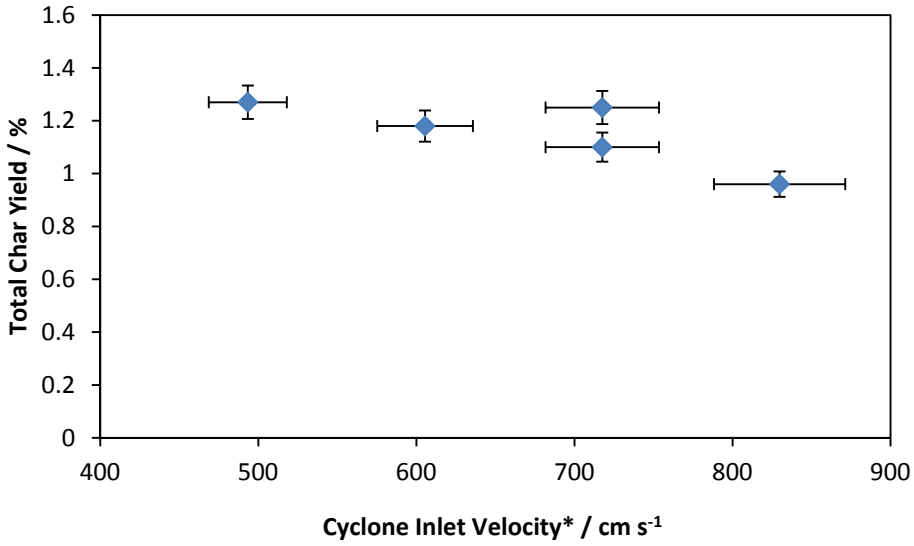

* at preheat temperature = 400 ºC and pyrolysis pressure = 4.5 bar

Figure 1.12: Variation of char yield with inlet velocity with the prototype cyclone-type fast-pyrolysis reactor

1.1.2.3 Conclusions

The experiments on the prototype, cyclone, fast-pyrolysis reactor were successful. The cyclone design was robust and prevented clogging of the biomass in the inlet section at sufficiently high gas velocities and with a proper gas pre-heating scheme. The reactor was also capable of high heat transfer rates to the biomass, which was deduced from the low char yield. Liquid yield increased with decreasing residence time through the reactor, which was rationalized by the hypothesis that the secondary decomposition reactions to permanent gases were minimized by decreasing vapor residence time in the reactor and transfer line. Not surprisingly, it was also possible to achieve some water/oil separation by condensing the liquids in two stages, a strategy that should be utilized in commercial applications of traditional pyrolysis reactors. Although some questions remain unanswered, the experiments have shown that this reactor design produced results that meet equipment requirements for future studies. These results have been used to design and build an optimized, cyclone-type, fast-hydropyrolysis reactor, which will be used for studies in H_2 at high pressure.

1.2 Design and Construction of a Cyclone-type, High-Pressure, Fast-Hydropyrolysis Reactor System

After successful completion of tests with the prototype, cyclone-type, fast-pyrolysis reactor, the results were used to design a new cyclone-type, high-pressure, fast-hydropyrolysis reactor system which is safe for use with hazardous gases. In parallel with reactor design and construction, preparations have been made with regard to safe use of hydrogen and carbon monoxide in the laboratory. Both aspects are described in detail here.

1.2.1 Apparatus Design

Overview

A 3-D representation of the new, cyclone-type, fast-hydropyrolysis (FHP) reactor, fixed-bed reactor, and condenser is shown in Figure 1.13. The process flow diagram for the system is shown in Figure 1.14. The main purpose of the FHP reactor is to perform fast-pyrolysis of biomass at high pressure and high temperature in a simulated coal gasifier effluent, hydrogen + carbon monoxide, atmosphere. The biomass enters the cyclone tangentially and is pyrolyzed on contact with the inner walls of the cyclone which are heated to ~500-550 °C. The char and hydropyrolysis vapors are separated by the cyclonic action of the reactor and by gravity. Char falls and accumulates in the char collector below the reactor, while vapors and permanent gases exit the though top of the cyclone and pass through the connector section to the fixed-bed catalytic reactor which will be used for vapor-phase upgrading studies. The connector section has two feed-throughs for temperature measurement or for inputting a quench gas to help decrease the vapor temperature just before the catalytic reactor, if needed. The effluent from the fixed-bed reactor then passes through a concentric-tube heat exchanger to condense vapor products. Permanent gases are then separated from the effluent of the heat exchanger in two stages. The first stage is comprised of a coalescence filter and the second is a cold-finger trap, cooled with a water/ice mixture, similar to the one used in the prototype cyclone reactor experiments Figure 1.9. After separation, permanent gases pass through a pneumatically-controlled, back-pressure regulator before being split into exhaust and gas chromatograph (GC) sampling streams. The FHP reactor and pre-heater section are heated via high-temperature laboratory heating tape and covered with fiberglass insulation while the connector section and HDO reactor are heated and insulated with custom-made heating jackets.

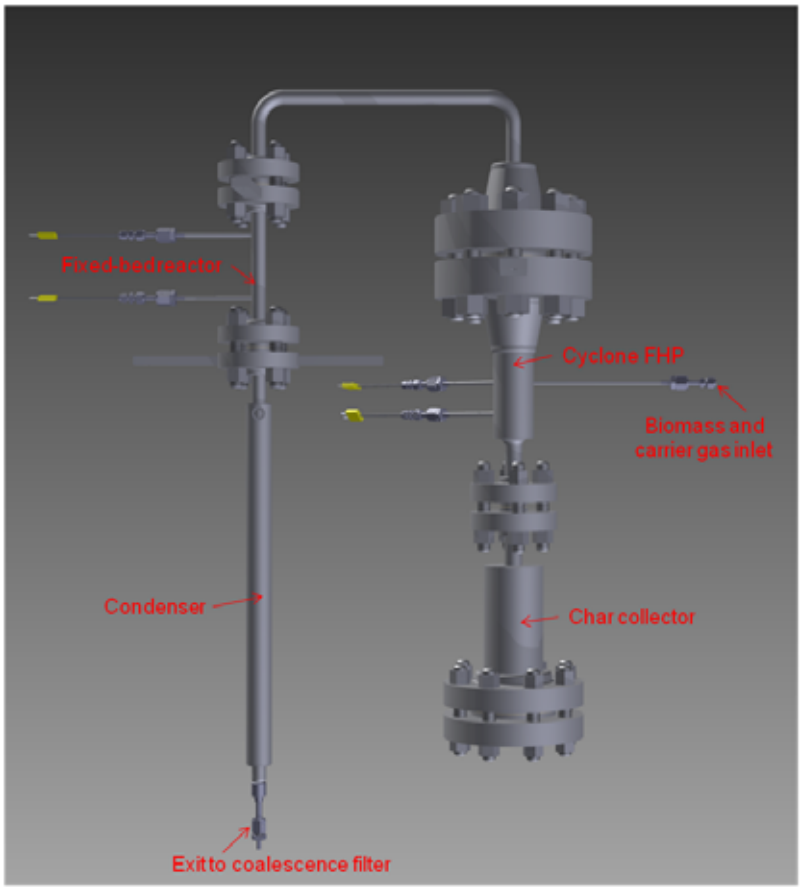

Figure 1.13: Computer representation of the cyclone-type, fast-hydropyrolysis reactor

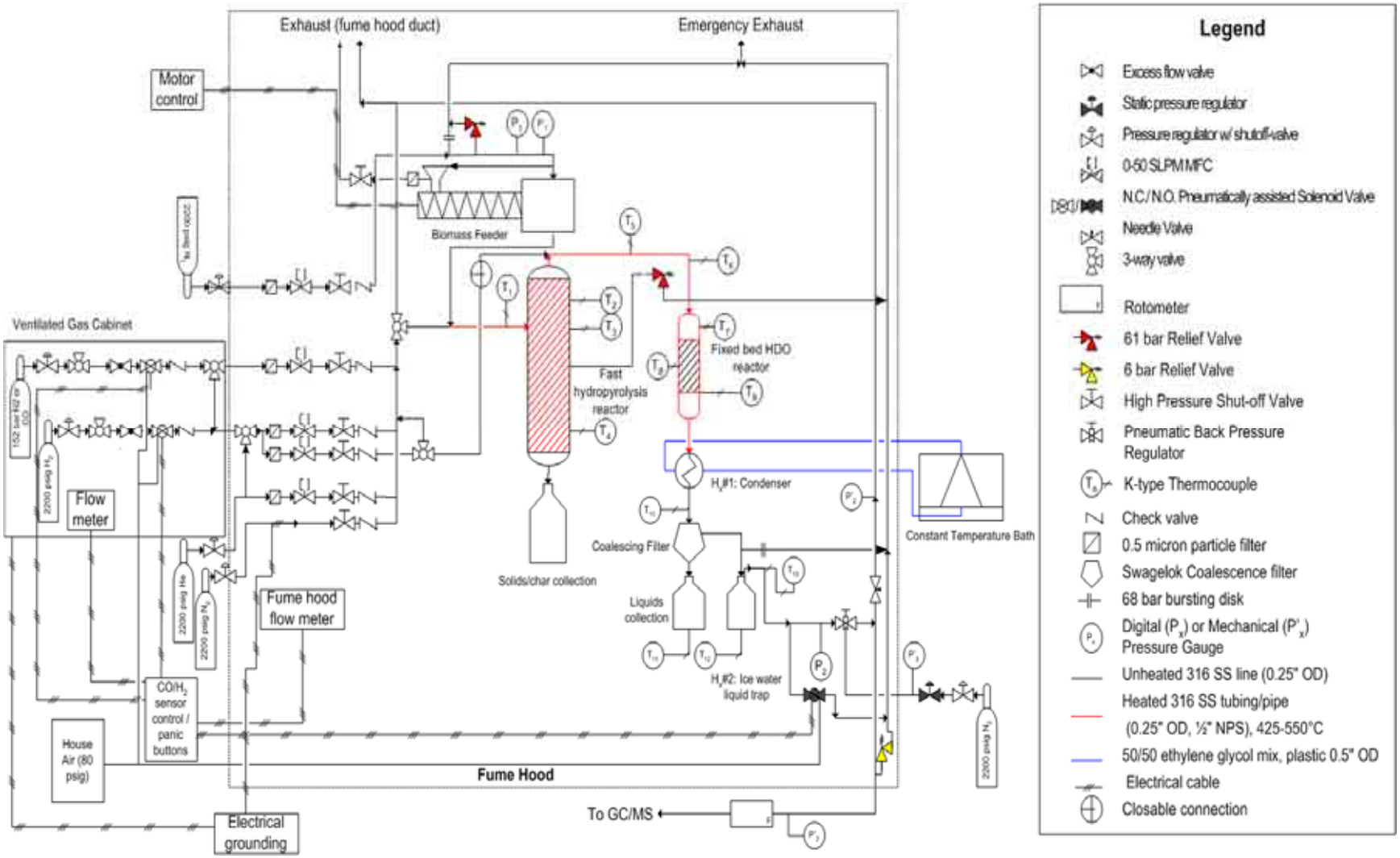

Figure 1.14: Process flow diagram for the high-pressure cyclone-type FHP reactor system.

Design Details

The cyclone-type, FHP reactor, shown in Figure 1.15, has been designed for pressures up to 100 bar and wall temperatures up to 650 °C in a H_2/CO atmosphere. Two feed-throughs welded to the reactor body are used to monitor inner wall temperatures and for emergency pressure relief. The internal dimensions of the reactor have been decreased slightly compared to the prototype cyclone reactor to reduce vapor residence time and improve overall strength. Flange connections and wall thickness are based on ASME B16.5 flange standards and B31.3 process piping codes. The material of construction used is high-alloy stainless steel to avoid loss of structural integrity due to hydrogen embrittlement and corrosion. The body of the cyclone reactor was machined from stainless-steel 347 round bar and has an OD of 2.375" and ID of 1.69", corresponding to schedule 160 pipe. At 650 °C, the basic allowable stress for TP347 seamless pipe is 4,400 psi (5,900 psi at 600 °C) which corresponds to an internal design gage pressure of 110 bar (or 145 bar at 600 °C).

The flange connection at the top of the reactor is a F316H 2" #2500 B16.5 flange, which has a maximum working pressure of 106.5 bar at 650 °C. At the bottom of the reactor, the OD and ID are 1.05" and 0.614" respectively, which corresponds to schedule 160 pipe and has an internal design gage pressure of 179 bar. The bottom flange which is used to connect to the char collector is a F316H #1500 ¾" B16.5 flange, which has a maximum working pressure of 106 bar at 593 °C. All the flanges are secured using ASME B8M-class 2 studs and stainless-steel 316 nuts and washers lubricated with a nickel-based lubricant. The feed-throughs and feed inlet have Swagelok VCR connections.

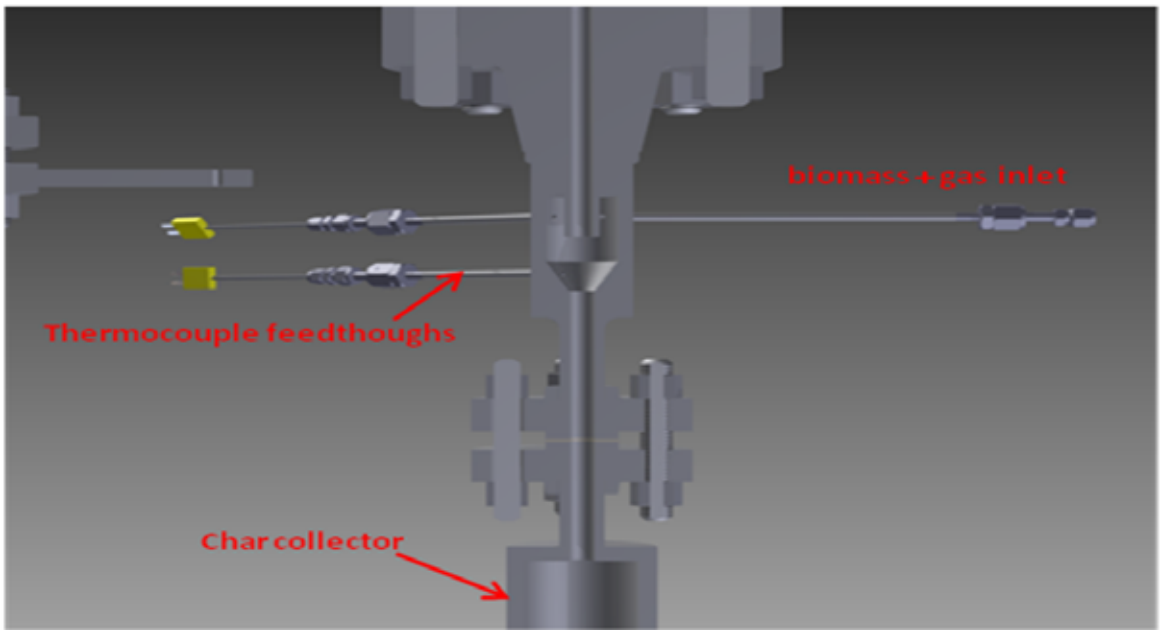

Figure 1.15: 3-D half section view of the cyclone-type fast-hydropyrolysis reactor

The char collector for the FHP reactor was designed based on the char collector for the prototype reactor. The collector is appropriately sized to contain several hours' worth of char and catalyst, if it is co-fed to the reactor at a rate of 1 g min^{-1}. The char collector is machined from stainless-steel 316 round bar and has

an OD of 3.5" and an ID of 2.626", equivalent to schedule 160 pipe. At 315 °C, the char collector body has an internal design gage pressure of 381 bar. The bottom of the collector uses F316H #600 3" B16.5 flanges for access to the inside of the collector, if needed. These flanges have a maximum working pressure of 100 bar at 40 °C.

The fixed-bed catalytic reactor, Figure 1.16, consists of a 6" long empty tube with a catalyst-bed support mechanism welded near the bottom. This reactor has been designed for pressures up to 100 bar and temperatures up to 500 °C in an H_2/CO atmosphere in order to test hydrodeoxygenation and water-gas-shift catalysts. Two thermocouple feed-throughs welded to the reactor body allow measurement of the temperatures of the inlet vapor and the catalyst bed. The reactor body is made from ½" schedule 80 A312 TP316 piping and socket-welded to F316H #1500 B16.5 flange connections. The pipe has an internal design gage pressure of 236 bar at 650 °C. The flanges have maximum working pressure of 106 bar at 593 °C. The connector from the cyclone reactor to the secondary reactor is made from ½" schedule 80 A312 TP316 piping and uses ½" F316H #1500 and 2" F316H #2500 B16.5 flange connections. These flanges have a maximum working pressure of 132 and 106.5 bar at 650 °C respectively.

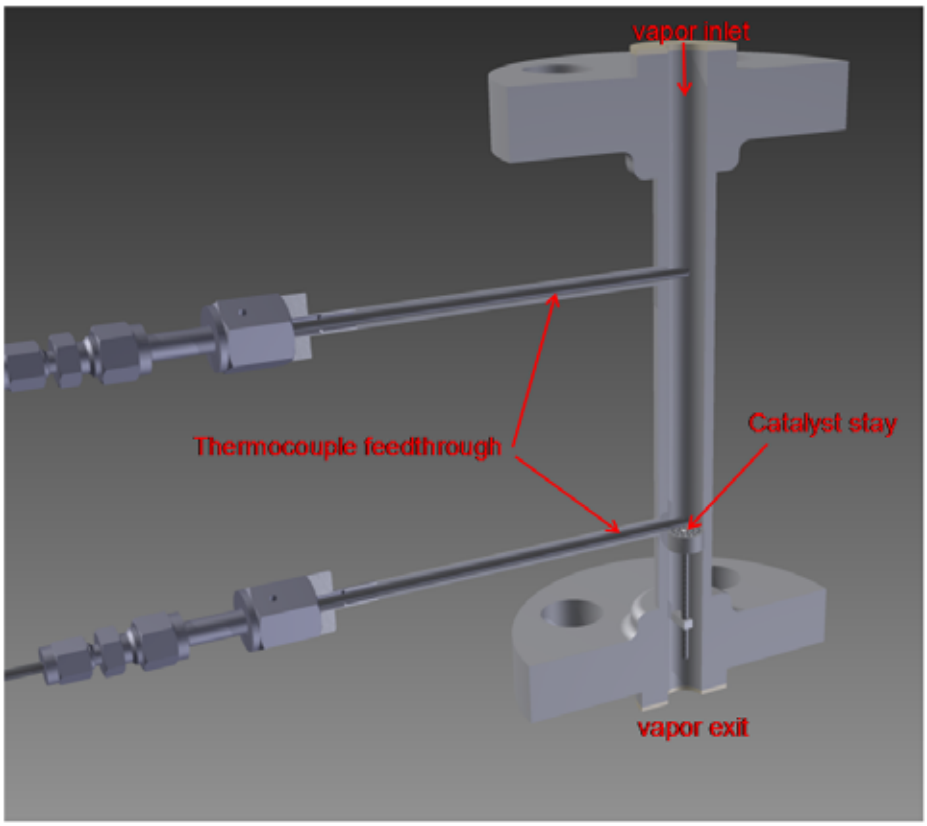

Figure 1.16: 3-D half section view of the fixed-bed catalytic reactor

The 20" long heat exchanger was sized based on heat transfer correlations and consideration of the prototype cyclone reactor experimental data. The heat exchanger is cooled to 5 °C with a 50/50 ethyl glycol and water mixture chilled and circulated by a 1 kW chiller. The tube portion of the shell and tube

condenser is made from schedule 80 A312 TP316 piping and connects to the fixed-bed reactor (or, if the that reactor is not used, to the connector from the cyclone reactor outlet) with a ½" #1500 B16.5 flange. The pipe has an internal design gage pressure of 236 bar at 650 °C. The flange on the top has a maximum working pressure of 106 bar at 593 °C. The exit of the condenser connects to the coalescence filter via ¼" A312 TP316 tube with a wall thickness of 0.028" welded to a ¼" Swagelok fVCR connector which has a maximum allowable working pressure of 275 bar at 100 °C.

The reactor system will be monitored and controlled by computer using custom-made Labview Compact-Fieldpoint hardware with real-time capabilities (cFP-2220), Figure 1.17, and Labview 2009 software package. The system pressure, temperatures in various sections of the reactor and other heated zones, and flowrates of biomass and gas into the reactor system can all be monitored, recorded, and/or controlled. The Labview system also provides visual and audible high and low alarms for various temperatures and pressures to warn the operator of any deviation from the desired operating conditions.

Figure 1.17: Labview hardware for process monitoring/control and data acquisition.

Process Safety

Several redundant safety systems have been incorporated into the reactor system design in order to deal with the inherent danger of operating at high pressures, high temperatures, and with hazardous gases like H_2 and CO. To protect the system from over-pressurization, the reactor has pressure relief devices upstream and downstream of the reactor as well as on the reactor itself. All the pressure relief and rupture disks are connected to a ¾" stainless-steel emergency vent line which vents directly outside on the roof of the building. The possibility of over-heating in each heating section is reduced by automatic power shutoff coding in the Labview software and by manual switching, if needed.

An active, process and laboratory safety system which relies solely on analog circuitry has been incorporated to automatically shut down the reactor in case of a leak or emergency. Four sets of H_2 and CO detectors are strategically placed in the hood and lab space to monitor for any leaks. A hood flow

monitor insures that adequate ventilation is being provided by the fume hood. If a leak of H_2/CO is detected, or exhaust flow in the hood slows or stops, or if the operator presses the "panic button", the system automatically stops flow of flammable gases through normally-closed solenoid valves, depressurizes the reactor system through a normally-open solenoid valve connected to the emergency vent line, initiates a reactor purge with inert gas, and cuts off power to the heaters. As a last defense, a level-1, bullet-resistant, ¾" thick, polycarbonate shield is present in front of the reactor system to protect the operator in case of a catastrophic failure of equipment.

1.2.2 Progress on Construction

The reactor system is in the final stages of construction. All the raw materials required for the reactor have been acquired, machined to specifications, and are currently being welded together and assembled. In parallel, a safety review for the complete reactor system was conducted with experienced research personnel with relevant experience with hydrogen systems. A hazards and operability study (HAZOP) for the complete reactor system and standard operating procedures were completed and reviewed.

After the construction of the reactor, it will be tested at high-pressure in an inert atmosphere before completing a final safety review. Once both tasks are complete, experiments based on tasks outlined in Year Three work will begin.

1.3 Fundamental Studies of Fast-Pyrolysis and Fast-Hydropyrolysis

To reach the ultimate goal of achieving fast-hydropyrolysis (FHP) of biomass, it is necessary to design a hydropyrolysis reactor with the optimal parameters to produce, selectively, a consistent bio-oil that can be easily handled and quickly upgraded. One of the key variables in the design of this reactor is the rate at which the biomass is heated.

Because of the difficulty of elucidating and controlling key variables which affect the quality of oil produced from FHP using traditional, lab or pilot-scale reactor systems, a micro-scale apparatus was designed and built which allows us to perform in-depth, fundamental studies. Using this apparatus, experiments aimed at studying the effect of heating rate on the unwanted char by-product during pyrolysis using cellulose as a model feedstock have been completed. The results are presented here.

1.3.1 Experimental Methods

Experiments were conducted in one of two custom, six-sided, stainless-steel, micro-reactor chambers with internal volumes of roughly 0.4 L and equipped with borosilicate viewports to allow for monitoring of the reaction, as shown in Figure 1.18. The two reactors differed only in their maximum operating pressures. Biomass heating was performed using a Pyroprobe (Pyroprobe 5200, CDS Analytical, Oxford, PA), which consists of a resistively heated platinum ribbon approximately 2.1 mm x 35 mm x 0.1 mm.

Cellulose particles with a mean diameter of 50 μm were loaded onto the surface of the Pyroprobe, which was inserted into the chamber through a modified 2¾" flange, and the system was flushed with inert gas to remove any oxygen. The particles were held in place by electrostatic interactions with the surface in a

way that prevents agglomeration or vertical stacking of particles. This procedure is a key element of the experiment, as heat transfer to the sample is critical, and a thick layer of sample would result in thermal lag and uneven heating of each individual particle. The intimate solid-solid contact represents the ideal heat transfer scenario and, coupled with the ability to heat the samples at rates up to 20,000 °C s^{-1}, makes this system a much better candidate for studying the fundamentals of fast pyrolysis than a typical thermogravimetric analysis (TGA) experiment.

The cellulose samples were heated at rates representing one of three different regimes: slow, TGA-type heating (15 °C min^{-1}), intermediate heating typical of pyrolysis (200 °C s^{-1}), and the maximum possible rate (20,000 °C s^{-1}). The gas atmosphere was also varied to determine the effects of reaction environment. Experiments were conducted at 1 bar He, 1 bar H_2, and 30 bar He. In each experiment, the ribbon was heated to a final temperature of 600 °C, where it was held for 1 s before being allowed to cool back to room temperature. Pictures of the platinum ribbon were taken using an optical microscope (Olympus BX51, Olympus, Central Valley, PA) before introduction into the chamber and after reaction in order to determine the degree of char formation.

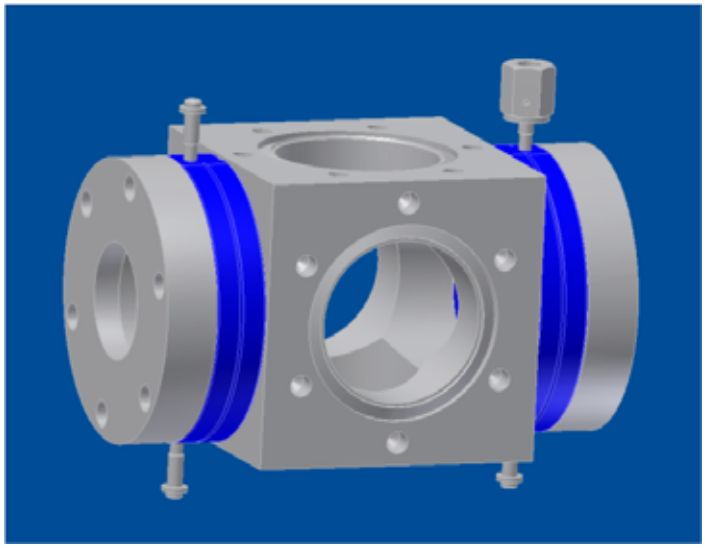

Figure 1.18: CAD drawing of the six-sided micro-reactor with two high-pressure borosilicate viewports.

1.3.2 Results and Discussion

The approximate amount and type of char formed at a given heating rate were similar at all three pressures. Heating the cellulose at 15 °C min^{-1} resulted in a significant amount of char formation, as shown in Figure 1.19. Similar amounts of char formed after pyrolysis in atmospheric pressure helium and hydrogen at the same heating rate. The following hypothesis is consistent with the results. At a low heating rate, cellulose slowly decomposes on the surface and forms amorphous carbon structures with a high C:H ratio rather than forming lower molecular weight vapor and gaseous products. While some lighter compounds are inevitably formed, a large proportion of the original sample remains on the surface in the form of char.

Cellulose has a very ordered and regular structure, consisting of thousands of dehydrated glucose building blocks linked into long chains with little or no branching. In real biomass, however, cellulose corresponds to only around one-third of the mass, with the rest made up by hemicellulose (essentially a branched and lower molecular weight polymer made up of a variety of sugar monomers) and lignin, an amorphous, cross-linked set of molecules so random in its size and structure that no accurate model has been developed. If such a low heating rate causes the simplest of compounds found in plants to extensively char, then surely the yields of vapor products from real biomass would be unacceptable.

An interesting result was obtained by heating the cellulose at a rate of 200 °C s^{-1} in that the char formed droplets, which left "char rings" on the surface, as shown in Figure 1.20. This observation is consistent with and confirms the phenomenon reported previously, [1.6] which showed cellulose liquefying and bubbling off the surface during pyrolysis. This heating rate, then, corresponds to a transition zone for this particle size where the heating is fast enough to allow sufficient heat transfer throughout the particle to liquefy the sample. However, the heating is still not fast enough to completely volatilize everything, resulting in the ring of char. This heating rate can be regarded as the minimum order of magnitude required for an ablative reactor to efficiently pyrolyze cellulose, since the liquefied cellulose will "stick" to the surface upon contact, and can spread out on the hot surface, resulting in a larger contact area and smaller thermal lag through the sample. A reactor operating at lower heating rates relies on the contact of an irregularly-shaped solid particle with a hot surface, which would lead to less efficient heat transfer.

A heating rate of 20,000 °C s^{-1}, two orders of magnitude greater than the previous one, is fast enough to cause essentially complete vaporization of the samples. Consequently, the experiments at this heating rate resulted in virtually no char being formed, Figure 1.21. While this heating rate may be difficult to obtain in a large-scale reactor, it shows that it is possible to eliminate the formation of char for simple model biomass systems.

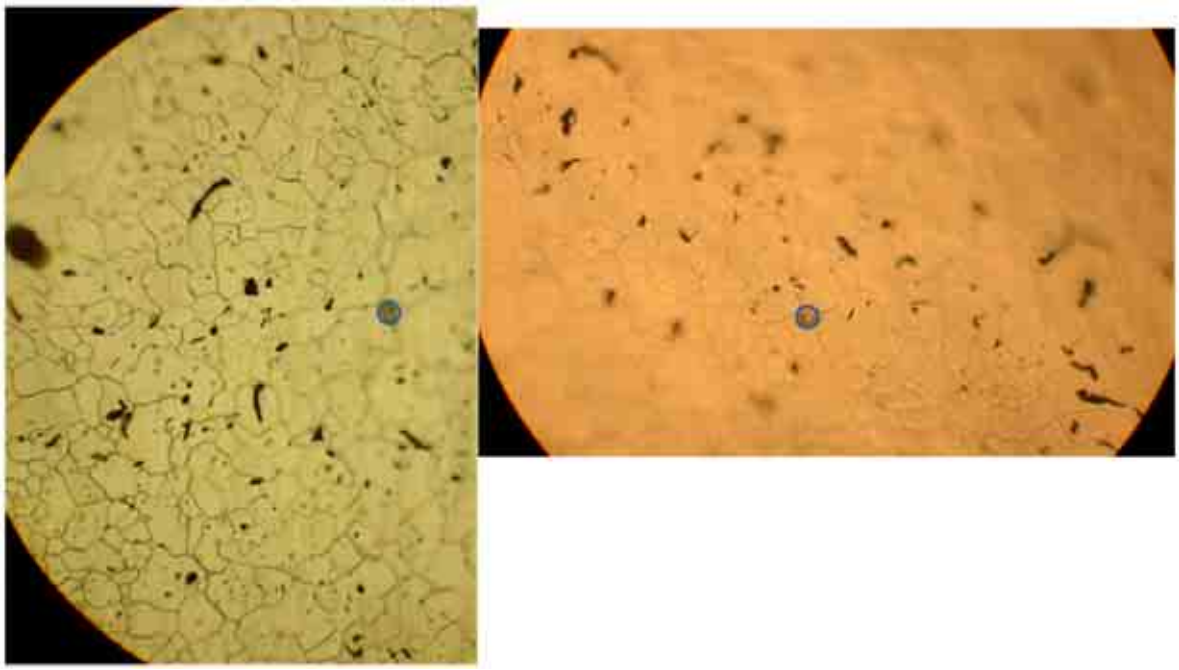

Figure 1.19: Char formed after 50 µm cellulose particles were pyrolyzed in 1 bar H_2 (left) and 1 bar He (right) at a heating rate of 15 °C min^{-1}. 20x magnification. The blue circles outline the same position on the platinum ribbon.

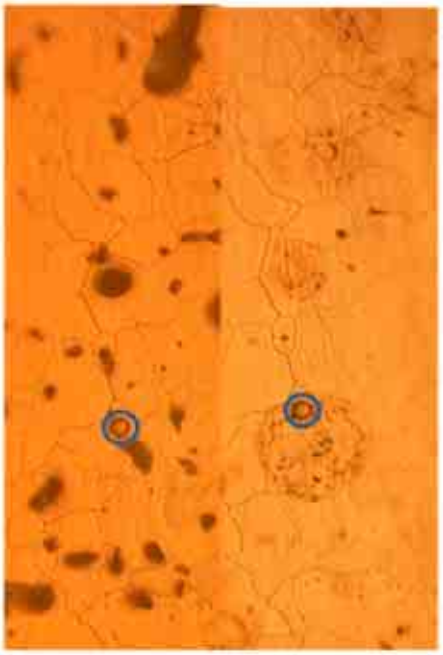

Figure 1.20: 50 µm cellulose before reaction (left) and after pyrolysis in 1 bar He at a rate of 200 °C s^{-1} (right). 20x magnification. The blue circle outlines the same position on the ribbon.

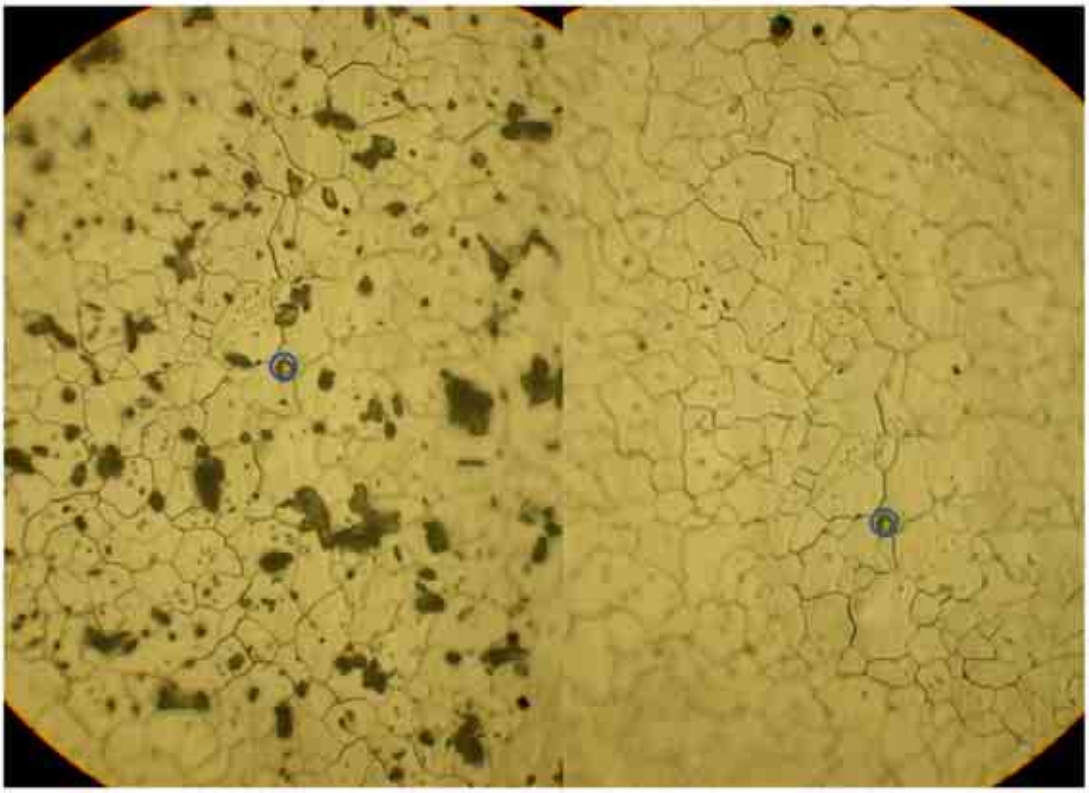

Figure 1.21: 50 µm cellulose particles on the surface of platinum ribbon (left). Char formed after pyrolysis in 1 bar H_2 at a heating rate of 20,000 °C s^{-1} (right). 20x magnification. The blue circle outlines the same position on the platinum ribbon.

1.3.3 Conclusions

The experiments that were conducted indicated the values of some of the critical parameters needed for design of a large-scale pyrolysis reactor. It was observed that for cellulose, heating rates on the order of 1,000 °C s^{-1} were sufficient to eliminate the formation of char, regardless of reactive gas atmosphere. Furthermore, the experiments determined that a heating rate in the 200-500 °C s^{-1} regime may be sufficient for an ablative reactor to function, as this is the required rate to liquefy cellulose particles.

Ultimately, the goal of the project is to develop a biomass-to-fuels process which utilizes hydrogen generated by coal gasification to help make a stable, high-energy-density product. Although studies of this high-pressure environment await implementation of the necessary safety features, results from the micro-reactor suggest that it is unlikely that high pressure of hydrogen will have an effect on the formation of char. Hydrogen, however, may prove vital in preventing the pyrolysis vapor products from further reaction by aiding in the removal of oxygen from the product molecules. It is now necessary to conduct similar experiments with other components of biomass, mixtures thereof, as well as real biomass to determine the behavior of these more complex systems during pyrolysis.

1.4 References

[1.1] A.V. Bridgwater, G.V.C. Peacocke, *Renewable & Sustainable Reviews* 4 (2000) 1-73.

[1.2] M. Rhodes, *Introduction to Particle Technology*, 2008, New York: Wiley

[1.3] S. Li, S. Xu, S. Liu, C. Yang, Q. Lu, *Fuel Processing Technology 85 (2004) 1201-1211*

[1.4] J. Lede, *Industrial & Engineering Chemistry Research* 39 (2000) 893-903

[1.5] J. Lede, F. Broust, F. Ndiaye, M. Ferrer, *Fuel* 86 (2007) 1800-1810

[1.6] P. J. Dauenhauer, J. L. Colby, C. M. Balonek, W. J. Suszynski, L. D. Schmidt, *Green Chemistry* 11 (2009) 1555-1561.

2.0 Optically Accessible Gasifier

2.1 Experimental Investigation of Coal and Biomass Gasification using *In-situ* Diagnostics

2.1.1 Introduction

Coal gasification can be considered as a three step process: (1) volatile, low molecular weight hydrocarbons are released as the coal particles are heated; (2) volatiles combust in the presence of an oxidant; and (3) the remaining char is gasified via heterogeneous reactions. For char consisting mostly of carbon, the following reactions are thought to dominate [2.1]:

$$C + H_2O \rightarrow CO + H_2 \quad \Delta H = 131\,\mathrm{MJ/kmol}, \tag{2.1}$$

$$C + CO_2 \rightarrow 2CO \quad \Delta H = 172\,\mathrm{MJ/kmol}, \tag{2.2}$$

$$C + 2H_2 \rightarrow CH_4 \quad \Delta H = -75\,\mathrm{MJ/kmol}. \tag{2.3}$$

These heterogeneous char gasification reactions proceed much slower than devolatilization or the homogeneous gas-phase reactions. Therefore, characterization of the kinetics of the heterogeneous reactions is vital for the design of coal to liquid fuel systems, and is an important goal of this project.

Most fundamental studies on gasification kinetics have been conducted in small-scale batch-reactors or bed-reactor configurations [2.2, 2.3]. However, most industrial gasifiers are of the entrained-flow design where small particles are transported and reacted in a moving gas flow. Compared to alternatives, entrained-flow gasifiers typically have higher fuel-throughput, greater conversion efficiencies, and enhanced ability to inject dry and wet fuels [2.4-2.6]. Due to differences in fundamental heat- and mass-transfer mechanisms, considerable controversy exits on the use of the kinetic rates derived from small-scale batch-type or bed-type reactors for the development of entrained-flow reactor systems. In addition, most fundamental studies on coal/biomass gasification study devolatilization and gasification as two separate mechanisms. However, in commercial processes, the two mechanisms are not conducted in separate systems; rather, they occur simultaneously and are dependent on the reactor heating rates and pressure. Once again, the use of these mechanisms for design of large-scale industrial gasifiers may not be optimum. For this reason, it is necessary to study the kinetics and the evolution of the major species of interest in an entrained-flow gasifier where devolatilization and gasification occurs simultaneously. Finally, a large number of previous studies derive kinetics rates from indirect indicators such as the rate of solid mass decrease or equilibrium product analyses. In such methods, the evolutionary history of the major species of interest – CO, CO_2, CH_4, and H_2 – are neglected. Such knowledge is needed to optimize gasifier efficiencies – by increasing the CO yield and reducing required energy inputs.

To obtain gasification kinetics data that can be applied to the design of a large-scale coal to liquid-fuel process, the objective of this project is design a lab-scale entrained-flow reactor. This reactor should accommodate a variety of feedstocks, operate at various temperature and pressures, and enable in-*situ* diagnostics. Quantification of the gasification reaction rates will be achieved using laser diagnostics of the CO and H_2O species concentrations at different stages in the over-all gasification process. The studies

reported here investigate the reaction kinetics for coal gasification, and future studies will include biomass and/or biomass/coal mixtures.

Gasification of biomass feedstocks, or combination of biomass and coal, provides advantages related to decreased reliance on hydrocarbon sources and reduced overall CO_2 emissions [2.7]. However, design and construction of biomass gasifiers also entails fundamental challenges. Biomass is made up of polymeric chain linked porous material which may undergo expansion, surface area to volume changes, and surface reactivity changes which are much more complex compared to coal. Biomass gasification is further complicated by the diversity in feedstocks. For these reasons, this project develops rapid experimental techniques to estimate reaction kinetics, measure particle morphology pre- and post-gasification, and guide in the development of reaction models.

2.1.2 Experimental Arrangement

Fundamental studies of coal and biomass gasification are being performed in a laboratory scale entrained-flow gasifier. Table 2.1 outlines the operating conditions for this gasifier. These conditions have been selected to match the common operating conditions of industrial entrained-flow gasifiers and to achieve high carbon conversion based on the conclusions of a well-stirred reactor model outlined in the final report for the previous year of this project [2.8]. Steam is used as the gasifying agent. Due to faster kinetic rates, steam was selected from alternatives, such as oxygen, air or CO_2 [2.3, 2.8]. In addition, the use of steam bypasses the auto-thermal gasification pathway which is responsible for the production of large quantities of CO_2. Therefore, steam provides a controlled environment in which to investigate methods for reducing the process generated CO_2.

Table 2.1: Design conditions.

Operating Parameter	Value
Pressure \ MPa	1.0 - 1.3
Reactor temperature \ K	1100 - 1400
Coal flow rate \ g s^{-1}	0.4 to 0.6
Steam flow rate \ g s^{-1}	1.2 to 1.8
External heating power\ kW	15
Residence times \ s	~ 10-15

The gasification arrangement consists of six subsystems – an optically accessible entrained-flow gasification reactor, a hydrogen-oxygen steam generator producing high-pressure and high-temperature steam, a high-pressure coal/biomass-feeder, an external heater system, an inline gas-sample collector, and a multi-channel data acquisition and remote-control system.

A schematic outlining the operation of the gasifier arrangement is shown in Figure 2.1. Steam and pulverized coal/biomass are injected into the optically-accessible reactor as simultaneous top-down flows. Energy for the endothermic gasification reactions (Eq. (2.1) and (2.2)) is provided by the high-temperature steam and sustained by additional electrical heaters along the length of the reactor. Laser

diagnostics in the form of tunable-diode-laser-absorption-spectroscopy (TDLAS) is used to probe major gas-phase species and temperatures at multiple axial locations along the gasification reactor. Partially gasified coal/biomass particles are contained in an ash collection system at the reactor base. Gas products including synthesis gas exit the system via the exhaust line. A control valve on the exhaust line maintains a constant pressure within the gasification reactor. Finally, a multi-sample gas collection system is installed at the end of the exhaust line. The collected gas samples are analyzed using gas chromatography for species concentrations and are used to verify the laser-based measurements.

Instrumentation in the form of pressure transducers and thermocouples continuously monitor the conditions of all systems and flows. This multi-channel data-acquisition and control system enables remote operation from an adjacent control room. Figure 2.2 displays the gasifier reactor, the hydrogen-oxygen steam generator and the coal/biomass feeder in a test-ready arrangement, and figure 2.3 displays the control room containing the data acquisition and control systems. In the sections that follow, further details are given for each of the sub-systems.

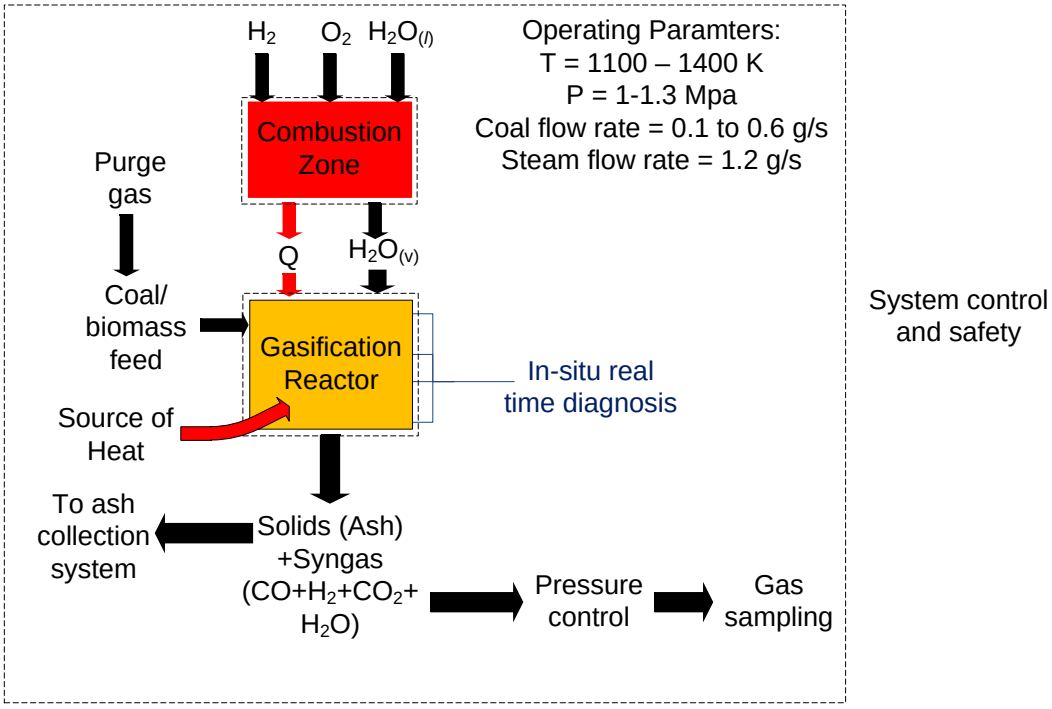

Figure 2.1: Schematic of the experimental operation.

Figure 2.2: Gasifier reactor, hydrogen-oxygen steam generator and coal/biomass feeder in the experimental test cell.

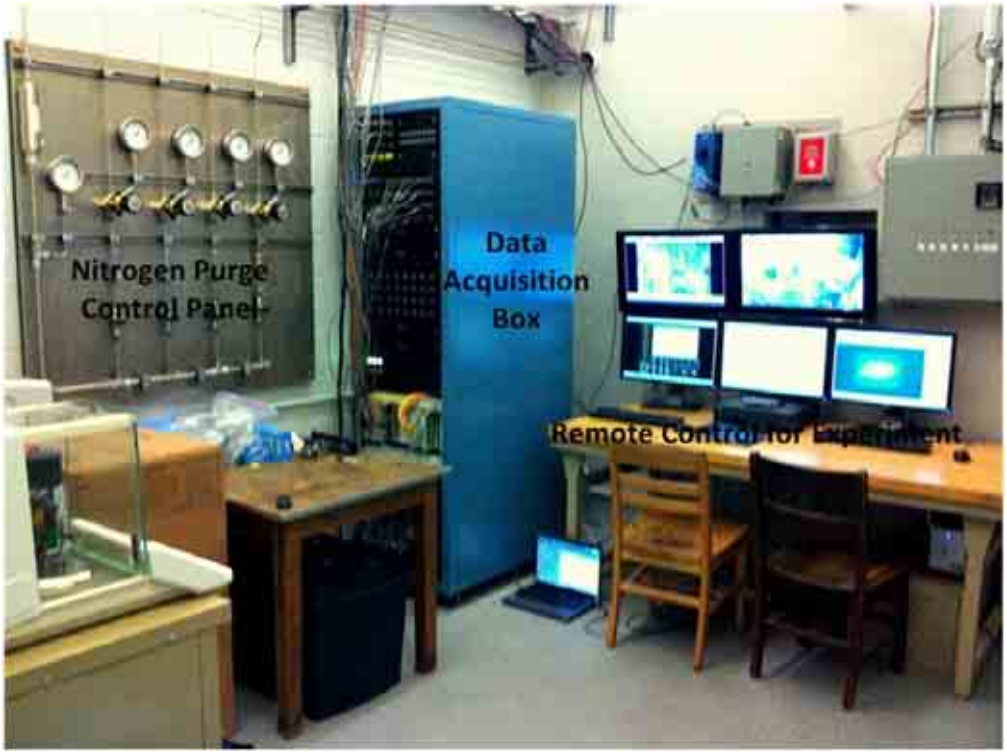

Figure 2.3: Nitrogen purge control panel, data acquisition and remote monitoring systems in control room.

2.1.2.1 Gasification Reactor Sub-assembly

The gasification reactor is constructed of stainless-steel 316 and has a height of 2.5 meters. The reactor consists of four interchangeable spool pieces each with an inner-diameter of 7.2 cm and wall-thickness of 2.54 cm. Figure 2.4 displays the physical reactor and its schematic.

During operation, high-pressure and temperature steam and coal/biomass are injected in the top-most spool piece. Mixing between the coal/biomass and steam is enhanced by a swirl-flow generated by the tangential injection of the steam into the reactor. Radiant heaters surround the spool pieces to provide 15kW of heat and sustain the endothermic gasification reactions. The large flanged-section at the bottom of the gasification reactor contains a dome for collection of ash and partially gasified particles. These particles are subsequently characterized using scanning electron microscopy (SEM). The system contains two pressure transducers and in excess of 20 thermocouples for temperature measurements.

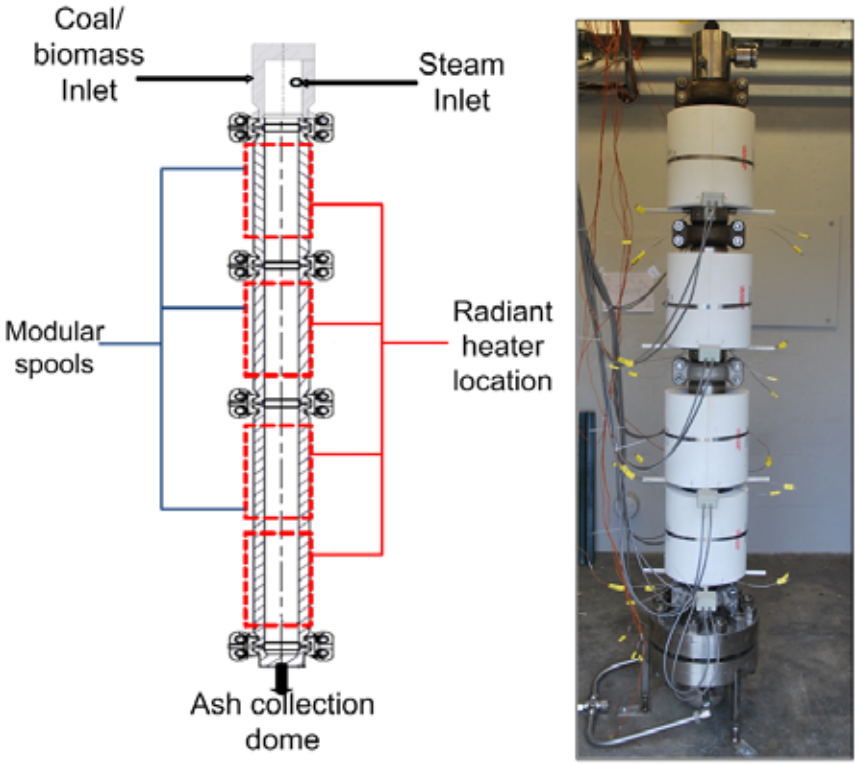

Figure 2.4: Gasification reactor schematic (left) and actual system (right).

2.1.2.2 Optical Diagnostics

In this investigation, tunable-diode-laser-absorption-spectroscopy (TDLAS) is being used for *in-situ* diagnostics of the gas phase temperature and species concentrations at multiple locations along the length of the entrained-flow reactor. Line-of-sight optical access for the TDLAS measurements is achieved using the optically accessible window section shown in Figure 2.5. Fused silica windows are assembled onto a spool-piece which can be interchanged with those shown in Figure 2.4. This allows for TDLAS measurements and flow characterization at four axial locations along the reactor, providing information

on the evolution of the major gas-phase species and reaction temperatures during the gasification progress.

Figure 2.5 displays the spool piece and its detailed schematic. The optical ports are sealed using grafoil gaskets and flanged connections. To prevent accumulation of solid particles on the window surfaces, the system includes a nitrogen manifold which maintains a continuous nitrogen purge across the optical windows. Tunable diode lasers with center wavelengths of 1388-nm and 2330-nm enable the measurement of the H_2O and CO species concentrations respectively [2.9-2.12]. This system has been fully leaked checked and has passed all preliminary tests.

The high-resolution transmission (HITRAN) molecular database was used to simulate absorption spectra of H_2O and CO. These calculations allow the selection of appropriate spectral region(s) for TDLAS measurements in the coal gasifier. Figures 2.6 and 2.7 show simulated CO spectra near 2.3 μm for a path length of 2.5 cm. Calculated spectra are shown at 300 K and 1100 K at pressures of 1 atm, 3 atm, 5 atm, and 10 atm. Few spectral transitions between 2.33 and 2.34 μm show sensitivity to temperature and have sufficient absorption at high temperatures. An appropriate central wavelength in this region will be selected for measurements of CO concentration in the coal gasifier.

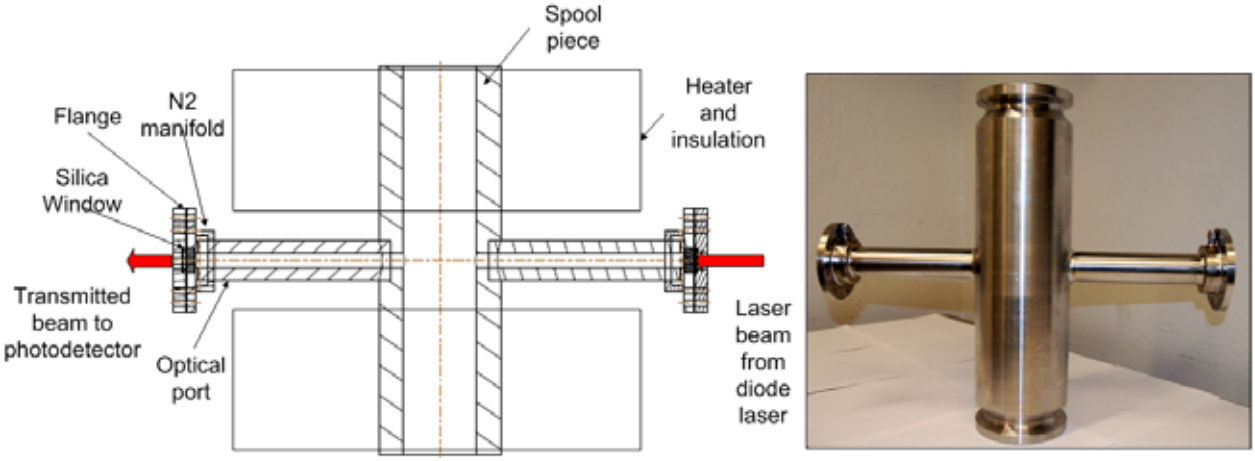

Figure 2.5: Schematic of the optical spool piece (left) and the actual hardware (right).

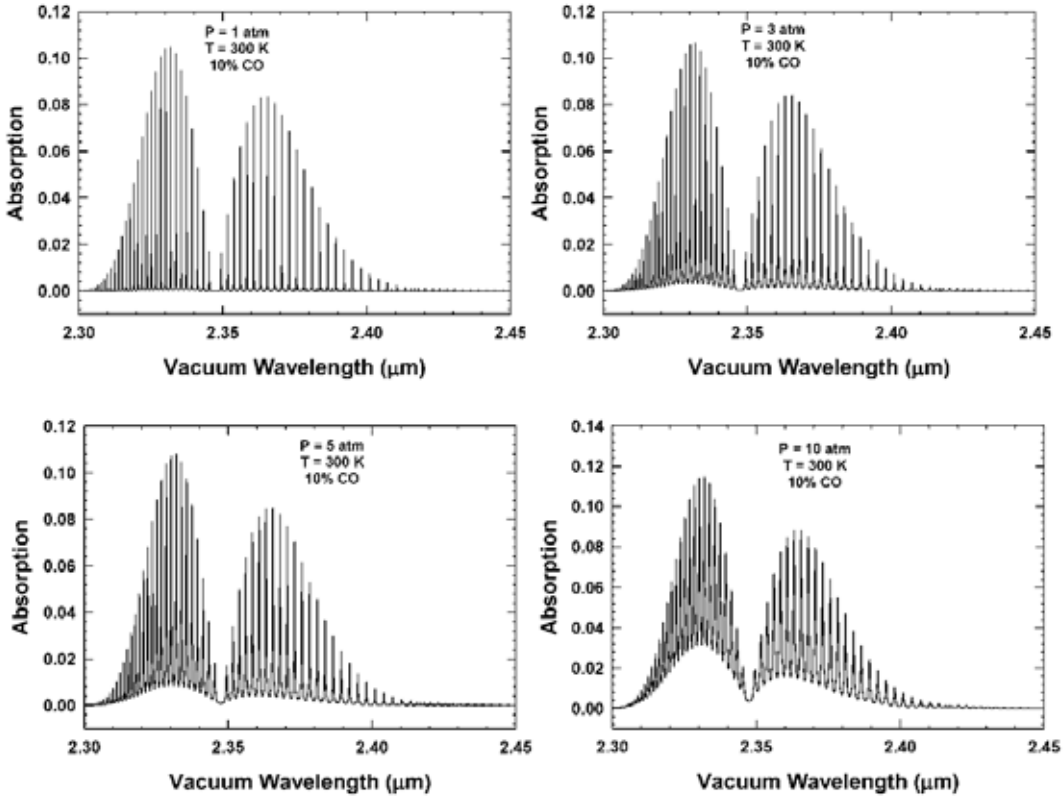

Figure 2.6: Calculated absorption spectrum of 10% CO near 2.3 μm at 300 K for four pressures in the range of 1 atm to 10 atm.

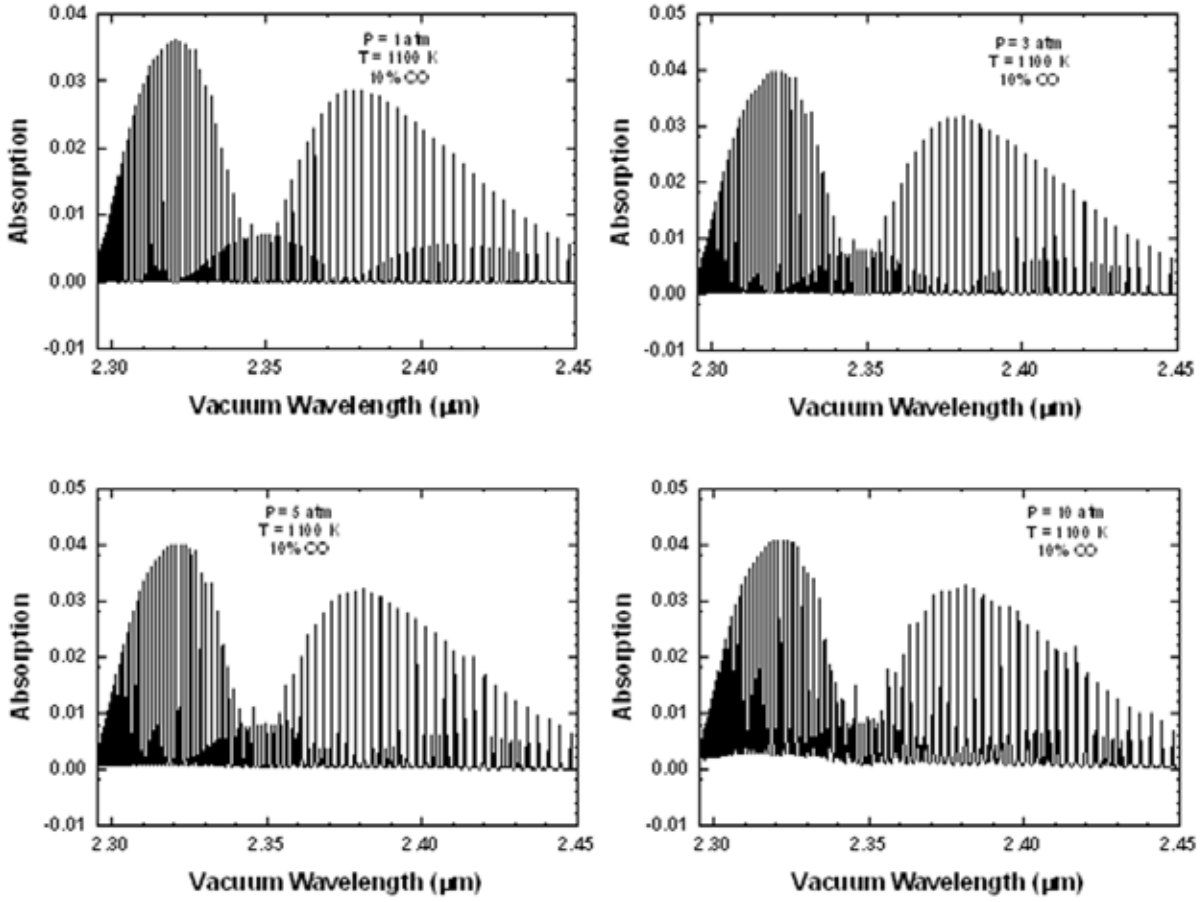

Figure 2.7: Calculated absorption spectrum of 10% CO near 2.3 μm at 1100 K for four pressures in the range of 1 atm to 10 atm.

2.1.2.3 Hydrogen-Oxygen Steam Generator

The hydrogen-oxygen steam generator was developed from concepts based on rocket combustors and is displayed with all reactant and product flows in Figure 2.8 [2.13-2.15].

Superheated steam (1100 to 1400 K) at high pressure (1.0 to 1.2 MPa) is produced inside the steam generator by quenching a H_2-O_2 flame. Hydrogen and oxygen inlets are located on the main casing and their mass flow-rates are controlled using sonic venturis. The entire oxygen flow and a portion of the hydrogen flow, termed core flow, are directed along the inside of the insert plug through a manifold. A fuel-lean pilot flame is formed inside the insert plug where initial ignition is provided by a spark plug. Typical equivalence ratios inside the insert plug range from 0.22 – 0.26. The remaining portion of the hydrogen flow, termed sleeve flow, is diverted through the annulus surrounding the insert plug. The sleeve flow surrounds the outer wall of the insert and provides cooling. At the end of the insert, the sleeve flow mixes with the pilot flame and forms the main H_2-O_2 diffusion flame. The global equivalence ratios for the main flame can be varied from 1.0 - 2.0 by adjusting the sleeve mass flow rate; thus the steam generator can be operated at fuel rich conditions with excess H_2 concentrations.

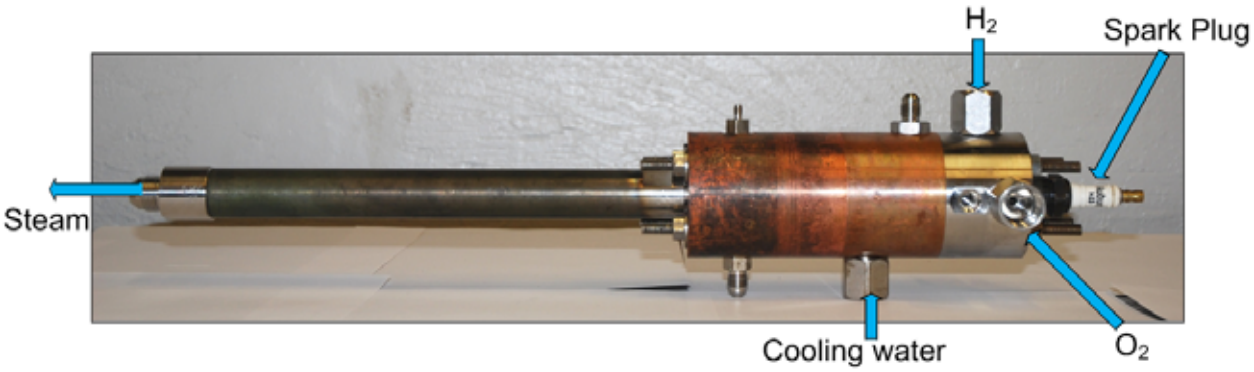

Figure 2.8: The hydrogen-oxygen steam generator.

Atomized liquid water sprays quench the main diffusion flame downstream of the main casing. The cooling water is injected into the main combustion chamber through micron-size orifices. The quenched flame passes through the interface piece that enhances mixing between the cooling water and flame. The connecting tube transports the steam from the interface piece to the gasification reactor. Finally, a sonic venturi located at the end of the connecting tube controls the steam flow-rate. The throat area of the sonic venturi was selected to ensure choked operation for all desired operating conditions.

Prior to instillation in the gasifier, experimental investigations were conducted to verify hardware reliability and assess the capability to meet the operating parameters shown in Table 2.1. Figure 2.9 shows the steam generator chamber pressure and steam temperature time history for the first 4 minutes of operation at stoichiometric operating conditions. Steady state conditions were achieved inside the steam generator after approximately 120 seconds. The initial spike in the steam generator temperature corresponds to ignition and flame propagation at low pressures. Rapid increases in pressure reduce the flame length which causes a subsequent reduction in temperature measured at the exit of the steam generator. Eventually, the reactor reaches steady state and near-adiabatic flame temperatures are achieved.

Figure 2.10 shows a comparison between calculated and measured thermodynamic properties (pressure and temperature) at steady-state conditions. The computations of the thermodynamic properties were done using an iterative method. The chamber pressure was calculated by starting with an assumed temperature for sonic condition at the throat. This calculated pressure was then used to recalculate the temperature based on adiabatic chemical composition. The iterations were continued until the error criterion was met ($e < 10\text{-}9$). For these calculations complete evaporation of liquid cooling water was assumed. The calculated temperature was assumed to be the stagnation temperature at the exit of the sonic nozzle.

The measured chamber pressures are in good agreement with calculated values. The chamber pressure is found to increase with increasing equivalence ratios. This increase is attributed to the increased mass flow rates inside the chamber due to greater hydrogen mass flow rates. The steam temperature was measured using a thermocouple located at the end of the connecting tube at atmospheric pressure. This measured temperature shows a good agreement with the calculated temperature at the throat of the sonic venturi.

These results verify operation of the steam generator meeting the design conditions outlined in Table 2.1. Following these experiments, the steam generator was installed onto the reactor vessel as shown in Figure 2.2. There it has been operated without incident for multiple long duration experiments (30 min each).

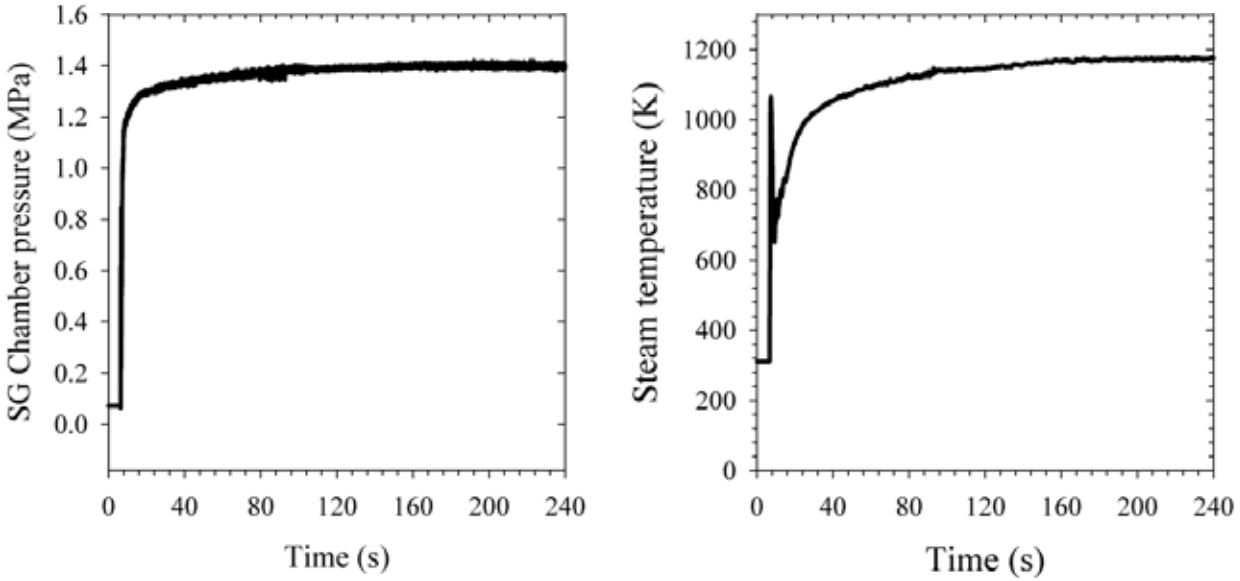

Figure 2.9: Steam generator chamber pressure (left) and steam temperature (right) time history for stoichiometric operation.

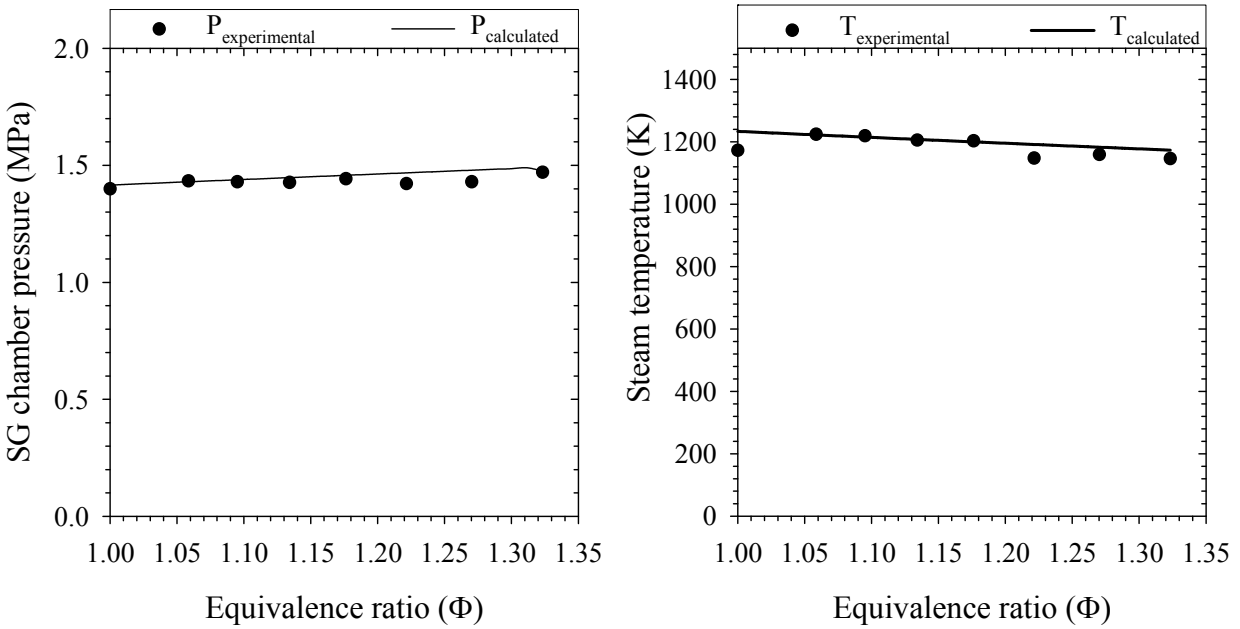

Figure 2.10: Comparison between experimental and calculated thermodynamic properties.

2.1.2.4 High-Pressure Coal/Biomass Feeder

A schematic and an image of the high-pressure coal/biomass feeder are shown in Figure 2.11. The feeder is based on a design described by Farias *et al.* [2.16]. This design enables injection of pulverized coal/biomass or coal/biomass slurries into the high-pressure gasification reactor. The mass flow-rates are metered by a motor-driven auger and carried into the reactor with a nitrogen purge. A pressure feedback line connects the end of the auger to the hopper, thus maintaining a zero-pressure gradient during the metering. The feeder is fixed to the gasification reactor and counter-weighted on a pulley system allowing it to rise when the gasifier reactor expands at high temperatures. Finally, a cooling jacket maintains the temperature of the coal/biomass at near-ambient conditions.

Figure 2.12 displays the mass flow-rate calibration curve as a function of the motor speed for Anthracite type coal. Similar curves have been derived for a variety of coals and biomass. The coals and biomass are typically ground to approximately 50-micron particle sizes. Slurry rheologies and granular-flow phenomenon determines the shapes of the curves.

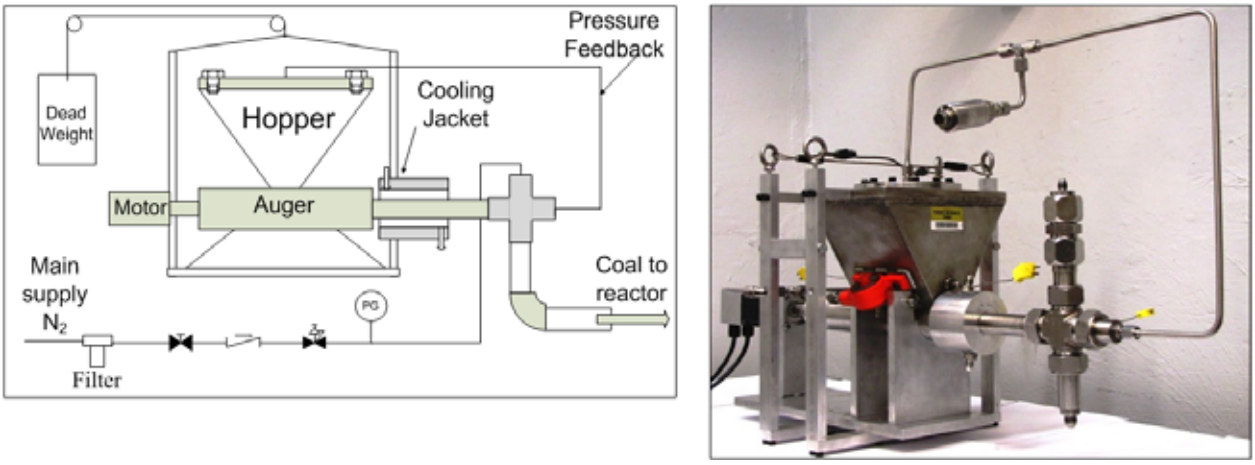

Figure 2.11: Schematic and image of coal/biomass feeder.

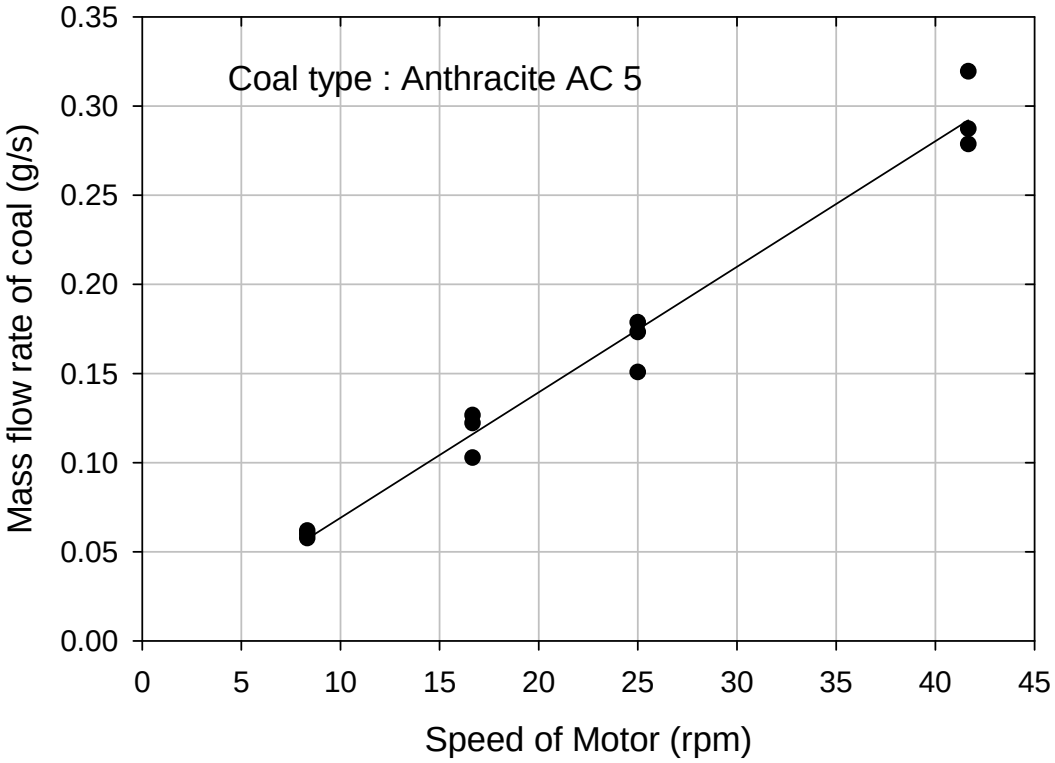

Figure 2.12: Coal flow-rate trend with motor speed.

2.1.2.5 Gas Sampling and Collection

Figure 2.13 displays a schematic of the gas sampling and collection system. This system contains a filter to remove solid particulates, a condenser and liquid-gas separator to remove water, and multiple sample collection cylinders to capture sample gases for analysis using a gas chromatograph. To collect a sample, the exhaust gases are diverted into a sample cylinder. Initially, the gases are allowed to flow through to purge the cylinder. Following this, the cylinder is sealed at the exit and gases accumulate within the cylinder until the cylinder pressure is equal to the reactor pressure. At that point, the gases within the cylinder are isolated using a shutoff valve, and exhaust gases are once again vented to the atmosphere. The current system enables collection of two gas samples during a gasification experiment. However, the system also includes the ability to accommodate a larger number of sampling cylinders if desired.

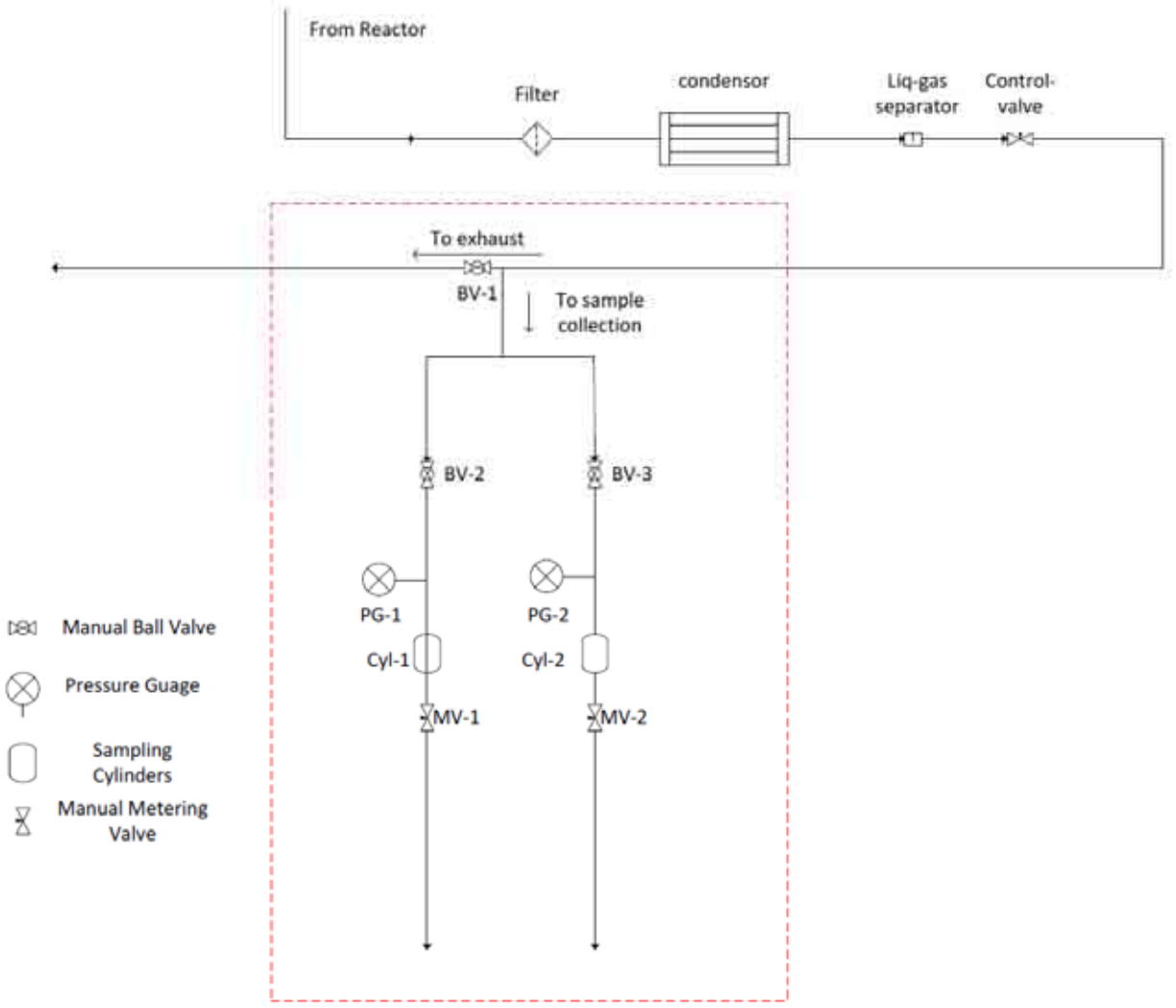

Figure 2.13: Schematic of the gas sampling and collection system.

2.1.3 Results and Discussion

Following design, construction, and calibration of all of the sub-components, the entire system was integrated for gasification experiments. At the start of such an experiment, the reactor is heated to the desired temperature using the radiant heaters. During the heat-up, the reactor is continuously purged with 0.4 g/s of nitrogen. The outer-wall temperatures of each spool piece as well as the gas-phase temperature within the reactor are continuously monitored using shielded thermocouples. Once the reactor temperatures reach the desired temperature, a gasification experiment is initiated.

The gasification experiment begins by ignition of the hydrogen-oxygen steam generator. This results in a rise in pressure and temperature within the steam generator as shown in figure 2.9. Within a few minutes, the steam generator achieves steady-state operation. At this point, coal is injected using the coal feeder shown in figure 2.11. Release of volatiles and gasification of the char causes an increase in the total

system pressure. Finally, the system pressure is slowly brought to the desired operating conditions by adjusting the pressure drop across a computer-regulated needle valve located in the exhaust stream. Once the system reaches steady-state operation, gas samples are collected using the sampling system shown in figure 2.13.

A number of initial gasification experiments have been performed. Gas chromatography of the collected gas samples has indicated the presence of carbon containing species including CO, CH_4, and CO_2, indicating gasification of the solid-phase carbon. Work is currently ongoing to verify experimental repeatability, implement TDLAS measurements, and study the hypothesis that gasification in an H_2 rich environment will reduce CO_2 formation.

2.2 References

[2.1] A. Williams, R. Backreedy, R. Habib, J.M. Jones, M. Pourkashanian, *Fuel* 81(5) (2002) 605-618.

[2.2] Nola G. D., Jong W. de, Spliethoff, H., 2010, Fuel Processing Technology, "TG-FTIR characterization f coal and biomass single fuels and blends under slo heating rate conditions: Partitioning of the fuel-bound nitrogen," 91, pp. 103-115.

[2.3] Niksa S., Liu G., Hurt R., 2003,"Coal conversion submodels for design applications at elevated pressures. Part I. devolatilization and char oxidation", Progress in Energy and Combustion Science, 29(5), pp. 425-477

[2.4] Hotchkiss, R., 2003, "Coal gasification technologies," Proceedings of the Institution of Mechanical Engineers, Part A: Journal of Power and Energy, 217(1), pp. 27-33.

[2.5] Guo X., Dai, Z, Gong X. et al., 2007, "Performance of an entrained-flow gasification technology of pulverized coal in pilot-scale plant," Fuel Processing Technology, 88(5), pp. 451-459.

[2.6] Minchener, A., 2005, "Coal gasification for advanced power generation," Fuel, 84(17), pp. 2222-2235.

[2.7] McKendry, P., 2001, "Energy production from biomass (part 1): overview of biomass," Bioresource Technology 83, pp. 37-46.

[2.8] Sane, A., Zheng, Y., Gore J., 2009, "A Study of Steam Gasification of Coal with CO2 using H2," Proceedings of the 6th U.S. National Combustion Meeting.

[2.9] Nagali, V., Herbon, J. T., Horning, D. C., Davidson, D. F., Hanson, R. K., 1999, "Shock-tube study of high-pressure H2O spectroscopy," Applied Optics, 38(33), pp. 6942-6950.

[2.10] Li H., Rieker G., Liu X., Jeffries J., and Hanson R., 2006," Extension of wavelength-modulation spectroscopy to large modulation depth for diode laser absorption measurements in high-pressure gases", Applied Optics, 45(5), pp. 1052-1061.

[2.11] Upschulte, B. L., Sonnenfroh, D. M., Allen, M. G., 1999, "Measurements of CO, CO2, OH, and H2O in room-temperature and combustion gases by use of a broadly current-tuned multisection InGaAsP diode laser," Applied Optics, 38(9), pp. 1506-1512.

[2.12] Wang, J., Maiorov, M., Baer, D. S., Garbuzom, D. Z., Connolly, J. C., Hanson, R. K., 2000, "In situ combustion measurements of CO with diode-laser absorption near 2.3 μm," Applied Optics, 39(30), pp. 5579-5589.

[2.13] G. Repas, 1994, "Hydrogen-Oxygen Torch Ignitor." NASA TM 106493.

[2.14] E. Dambach, D. Helderman., A. Boopalan.,T. Kite, 2006, "Spark-augmented Torch Ignitor Part I," Purdue University Internal Report, West Lafayette, IN, Spring 2006.

[2.15] A. Boopalan and D. Helderman, 2006,"Spark-augmented Torch Ignitor: Part II," Purdue University Internal Report, West Lafayette, IN, Fall 2006.

[2.16] Farias L., and Irons G.,1986, "A Pressurized Screw Feeder for Powder Injection", Metallurgical and Materials Transactions B, 17(1), pp. 229-231.

3.0 Flame Structure of Alternative Jet Fuels

3.1 Experimental investigation of flame structure using PIV

A comprehensive understanding of the flame structure of alternative jet fuels can be obtained using detailed measurements of velocity, temperature, and species concentrations in laminar, counter-flow flames stabilized in laboratory-scale burners. In the first year of the project, a new counter-flow burner with contracting nozzles was designed and fabricated for fully characterizing the velocity field in order to obtain rigorous comparisons between measurements and calculations of counter-flow flames.

Stereo particle imaging velocimetry (SPIV) measurements in laminar, non-premixed counter-flow flames were conducted. Figure 3.1 shows the SPIV system; the burner was enclosed to prevent the spread of seeding particles in the room. A frequency doubled Nd:YAG laser at a repetition rate of 15 Hz was used along with a TSI SPIV system. Only the oxidizer stream was seeded with alumina particles. A cyclone type seeder was used for seeding. The oxidizer input into the seeder was divided into two streams. One stream was introduced from the bottom of the seeder through a perforated piece of cloth whereas the other stream entered from the top and was injected via a tube just under the particle air interface. The synergistic actions of both the streams lead to particle entrainment in the output stream. A downside of this mechanism is the fluctuation in seeding density as the alumina particles around the particle air interface are swept into the exhaust stream. Periodic shaking of the seeder and cleaning of the flow lines was required to maintain uniform seeding density. Figure 3.2 compares the probability distribution of the size of alumina particles when they were left in the ambient for months and after they were heated in an oven kept at over 500 °C for several hours. As seen from Figure 3.2, the peak value of the size of the particles shifts from 6 μm to 2.5 μm for the heated particles. This can be explained due to desorption of water from alumina. Smaller diameter particles are expected to track the flow better because of less inertia. Heating of particles prevents clumping which leads to lower resolution as well as masking of small particles thereby reducing the number of particle pairs available for intensity cross-correlation.

Figure 3.1: Experimental SPIV system. The counter-flow burner is located inside the enclosure to avoid spreading of seed particles.

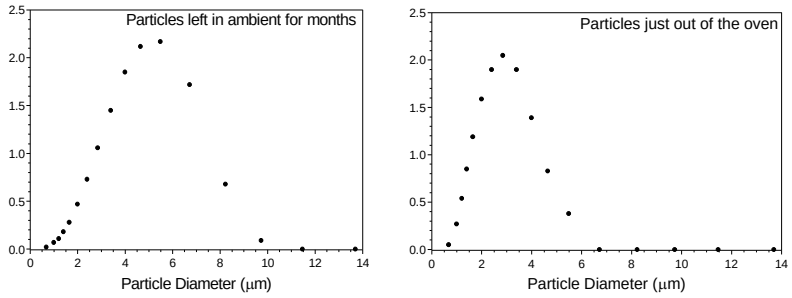

Figure 3.2: Probability size distribution (by volume) of alumina seed particles for SPIV. The peak of the distribution shifts from 6 μm to 2.5 μm for the heated particles.

The TSI system included two CCD cameras capable of frame straddling along with a synchronizer. Insight 6.0 software along with Tecplot was used for all post-processing of acquired data. The cameras were zoomed in to their highest magnification with f# of 5.6. A 4000 mm plano-convex spherical lens was used to collimate the naturally diverging beam to a 12 mm diameter beam and then a 1000 mm square cylindrical convex lens was used to narrow the beam asymmetrically to a sheet thickness of 900 μm. The pulse duration was 10 nanoseconds and energy per pulse was approximately 7 mJ. The repetition rate of the laser was 15 Hz which corresponds to 30 images being captured by each camera per second. The spatial resolution in the x-y plane was 34.59 μm/pixel by 34.59 μm/pixel and 900 μm in the z direction. Interference filters were used in front of the CCD cameras to suppress the low frequency background noise from flame emission and scattering from the counter-flow burner. The temporal spacing between the pulses should be small enough to capture adequate number of particle pairs (typically greater than 10) for cross-correlation but large enough to allow sufficient displacement of particles in order to minimize the error in the detection of the correlation peak. The temporal spacing (ΔT) between the pulses was maintained around 800 μs.

A single nozzle in isolation was studied with non-reacting gases in order to fully understand the effect of opposing nozzles in the counter-flow geometry. Figure 3.3 shows a sample SPIV image. The raw image indicates high quality of seeding density which is crucial for obtaining accurate velocity vectors. Figures 3.4 and 3.5 show the axial (y-direction) component of flow velocity at various axial distances from the nozzle exit. When seeding the oxidizer flow only from the bottom nozzle (Figure 3.4), the velocity profile is nearly symmetric about the central plane and is nearly flat for 3.5 mm on either side of the central plane i.e. nearly 70% out of the 10 mm nozzle diameter. On the other hand, the velocity profile is flat for 3 mm on either side of the central plane when seeding the oxidizer flow only from the top nozzle (Figure 3.5). The difference in the extent of flatness can be attributed to buoyancy effects. Figure 3.6 shows the variation of the z-component of velocity for the same axial locations when seeding the flow from only the bottom nozzle. The z-component fluctuates close to zero which indicates that the flow is nearly axi-symmetric.

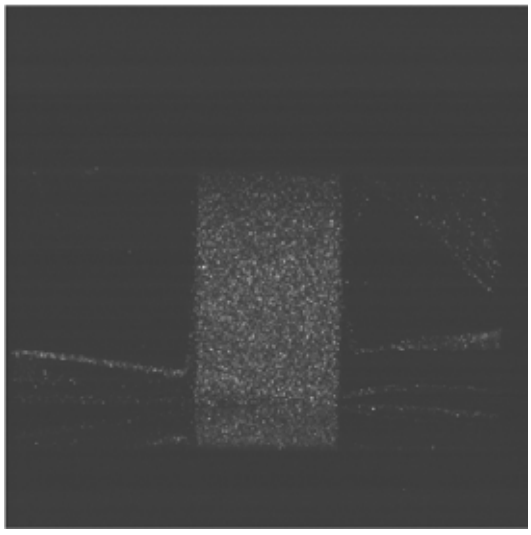

Figure 3.3: A raw SPIV image showing the sharp cut-off on top which indicates that the laser sheet was uniformly parallel to the bottom nozzle.

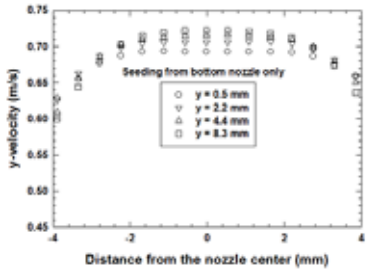

Figure 3.4: The variation of y-velocity (axial) at various axial distances from the bottom nozzle in a non-reacting mixture containing 21% O_2 (balance N_2), flowing at 2.83 slpm. The velocity is uniform over approximately central 7 mm (10 mm nozzle diameter). The flow was from bottom nozzle only.

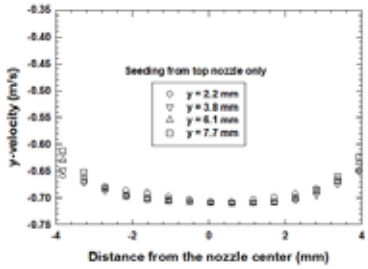

Figure 3.5: The variation of y-velocity (axial) at various axial distances from the top nozzle in a non-reacting mixture containing 21% O_2 (balance N_2), flowing at 2.83 slpm. The velocity is uniform over approximately central 6 mm (10 mm nozzle diameter). The flow was from top nozzle only.

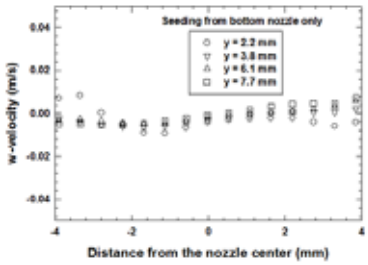

Figure 3.6: The variation of w-velocity at various axial distances from the bottom nozzle in a non-reacting mixture containing 21% O_2 (balance N_2) flowing at 2.83 slpm. The velocity fluctuates near zero indicating the flow is nearly axi-symmetric.

For reacting cases, varying levels of gaseous methane and nitrogen were used in the fuel stream while varying levels of gaseous oxygen and nitrogen were used in the oxidizer stream. The separation distance between the opposing nozzles was maintained at 12 mm for all measurements. The velocity of reactants was chosen to obtain a global strain rate of 100 s^{-1}. Figure 3.7(a) shows the axial (y-direction) component of velocity at various axial locations away from the nozzle exit with oxidizer (air) from the bottom nozzle and fuel (100% methane) from the top nozzle; while Fig. 3.8(a) shows the axial component of velocity at various axial locations away from the nozzle exit with oxidizer flowing from the top nozzle and fuel from the bottom nozzle. Figures 3.7(b) and 3.8(b) show the variation of the z-component of velocity for the same axial locations. The z-component fluctuates close to zero which again indicates that the flow is nearly axi-symmetric.

Measurements in counter-flow methane-air flames were also performed with varying dilution of nitrogen in both fuel and oxidizer streams. Figures 3.9 and 3.10 show the axial component of velocity at various locations for counter-flow flames containing 50% methane (diluted by 50% N_2 in the fuel stream) with various O_2/N_2 dilutions in the oxidizer stream. Compared to the methane-air flame (Figure 3.7(a)), the velocity profiles are affected with 50% O_2; but the effect appears to be similar with 75% O_2. With increased level of nitrogen dilution, the flow velocity reduces at comparable axial locations. There is also a marked decrease in the extent of the flatness of the velocity profile accompanied with a reduction in velocity at comparable axial locations.

Figure 3.11 shows the combined effect of varying levels of dilution and buoyancy on the particle distribution in the flow images. The change in flow curvature is noticeable as the percentage of methane is decreased in the fuel stream especially when the oxidizer is from the bottom. There is also a clear shift in the stagnation plane and location of the flame region as stoichiometry is varied. The seeding density decreases significantly as the particles enter the flame region. There is clearly more recirculation of the

flow when the oxidizer is from the top. It is unclear how much of the velocity change is due to factors such as the change in tracking ability of the particles, velocity bias in the measurements due to reduced seeding density, higher temperatures within the flame, the effect of temperature gradients in the flow field, or thermodynamic effect of particles on the temperature field. CARS temperature measurements in the same flames will be performed, and the temperature data will help resolve these questions.

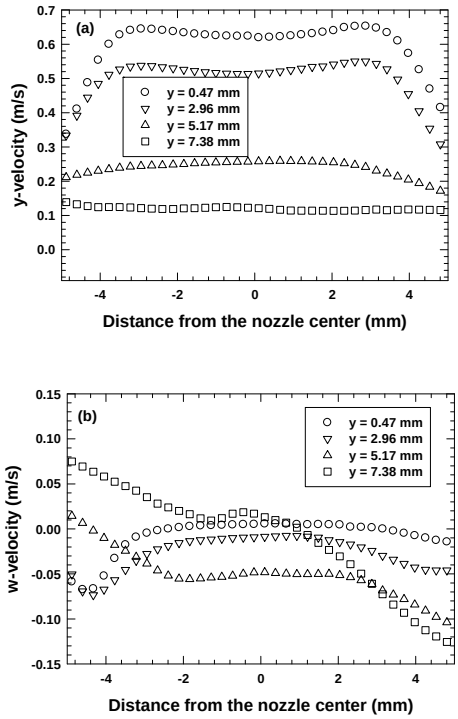

Figure 3.7: The variation of y-velocity (axial) at various axial distances from the bottom nozzle in a counter-flow flame at global strain rate of 100 s^{-1} containing 100% CH_4 in the fuel stream (top) and air in the oxidizer stream (bottom). The w-component fluctuates near zero indicating the flow is nearly axi-symmetric.

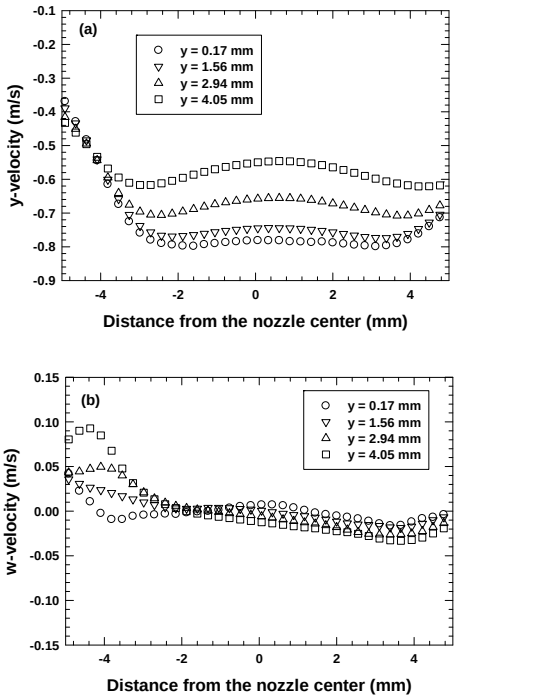

Figure 3.8: The variation of y-velocity (axial) at various axial distances from the top nozzle in a counter-flow flame at global strain rate of 100 s^{-1} containing 100% CH_4 in the fuel stream (bottom) and air in the oxidizer stream (top). The w-component fluctuates near zero indicating the flow is nearly axi-symmetric in the burner.

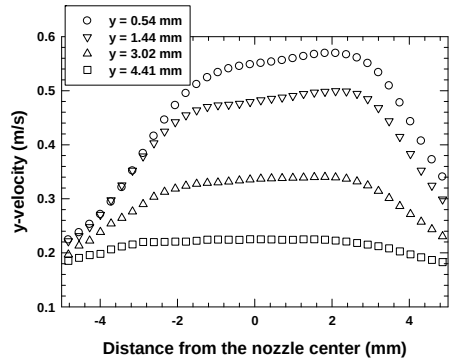

Figure 3.9: The variation of y-velocity (axial) at various axial distances from the bottom nozzle in a counter-flow flame at global strain rate of 100 s^{-1} containing 50% CH_4 (diluted with 50% N_2) in the fuel stream (top) and 50% O_2 and 50% N_2 in the oxidizer stream (bottom).

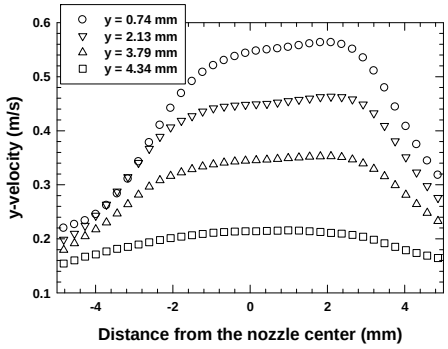

Figure 3.10: The variation of y-velocity (axial) at various axial distances from the bottom nozzle in a counter-flow flame at global strain rate of 100 s^{-1} containing 50% CH_4 (diluted with 50% N_2) in the fuel stream (top) and 75% O_2 and 25% N_2 in the oxidizer stream (bottom).

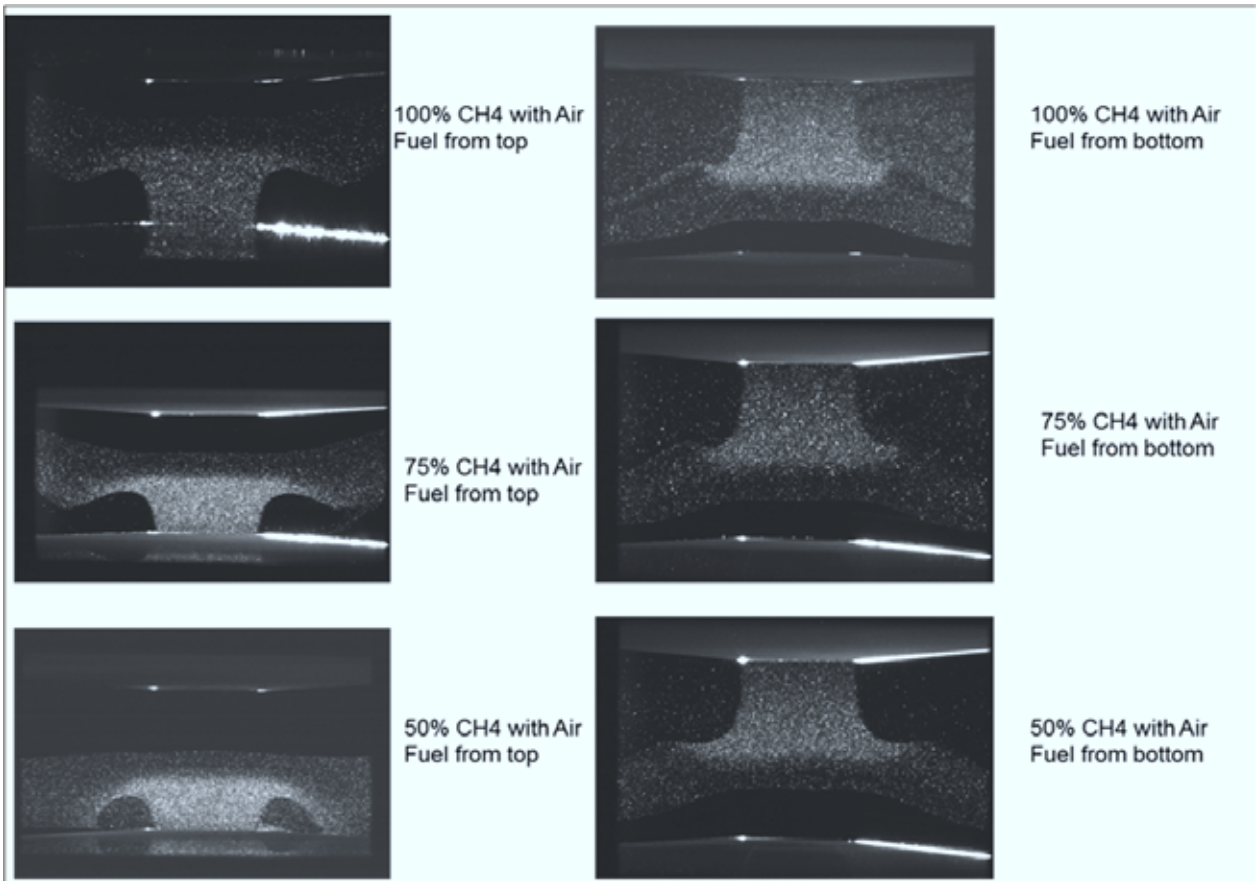

Figure 3.11: The change in particle seeding distribution due to coupling of buoyancy and change in the amount of nitrogen dilution in the fuel.

3.2 Numerical simulation of flame structure

Modeling studies of premixed and nonpremixed flames for major jet surrogate fuels were conducted, including n-heptane, and n-decane. These preliminary computational results as well as the experimental and computational data in literature indicate that large discrepancies exist in the predicted flame speed and flame structure using several different reaction mechanisms. Discrepancies also exist between predicted and measured flame speed, indicating flame speed comparison is not sufficient for evaluating current kinetic mechanisms and it is necessary to obtain accurate and detailed profiles of flame structure such as temperature and species concentrations. The CHEMIKIN code for 1-D premixed [3.1] and nonpremixed [3.2] flames was modified to handle several complex kinetic mechanisms for n-heptane and n-decane, respectively, including the JetSurF mechanism [3.3], a detailed chemical reaction model for the combustion of jet-fuel surrogate is being developed through a multi-university research collaboration funded by the AFOSR. The predicted flame structure will be compared later with the CARS measurements.

3.3 References

[3.1] R. J. Kee, J. F. Grcar, M. D. Smooke and J. A. Miller, A FORTRAN Program for Modeling Steady Laminar One-Dimensional Premixed Flames, Sandia National Laboratories, (1985).

[3.2] A. E. Lutz, R. J. Kee, and J. F. Grcar, "OPPDIF: A Fortran program for computing opposed-flow diffusion flames," Sandia National Laboratories, Report No. SAND96-8243 (1996).

[3.3] B. Sirjean, E. Dames, D. A. Sheen, X.-Q. You, C. Sung, A. T. Holley, F. N. Egolfopoulos, H. Wang, S. S. Vasu, D. F. Davidson, R. K. Hanson, H. Pitsch, C. T. Bowman, A. Kelley, C. K. Law, W. Tsang, N. P. Cernansky, D. L. Miller, A. Violi and L. R.P., JetSurF version 1.1, September, 2010.

4.0 Conclusions

The second year of the project involved manufacturing and utilization of apparatuses for biomass fast hydropyrolysis, hydrodeoxygenation, and gasification considered critical for the newly emerging synthetic fuel economy. Control of CO_2 emissions from these processes, as well as obtaining the highest overall energy and carbon conversion efficiencies, have been related opportunities. The specific conclusions from the present project are listed as:

(1) Proper design of the biomass feed inlet which prevents premature heating of biomass to temperatures below 100-200 °C is critical to the reduction of clogging in pyrolysis reactors.

(2) The prototype, cyclone, fast-hyropyrolysis reactor design was robust and prevented clogging of the biomass in the inlet section at sufficiently high gas velocities and with a proper gas pre-heating scheme.

(3) A second generation cyclone, fast-hyropyrolysis reactor that is capable of hydrogen service at high pressure was designed based on successful experiments with the prototype version of the reactor. The reactor is currently under construction.

(4) For cellulose, heating rates on the order of 1,000 °C s^{-1} are sufficient to eliminate the formation of char, regardless of reactive gas atmosphere. Furthermore, heating rate in the 200-500 °C s^{-1} regime may be sufficient for an ablative reactor to function, as this is the required rate to liquefy cellulose particles.

(5) Supercritical steam for gasification experiments can be reliably produced with an H_2-O_2 chemical steam generator which was based on modification of aerospace technology.

(6) The operation of the optically accessible gasifier capable of high-pressure and high-temperature experiments including varying levels of excess hydrogen has been verified with extensive sub-component and full system experiments.

(7) Tunable diode laser absorption spectroscopy measurements will provide in-situ diagnostics of temperature and gas phase species concentrations at multiple locations along the entrained-flow reactor. Initial measurements are expected soon.

(8) Spectral simulation of CO near 2.3 microns indicates transitions with temperature sensitivity for measurements in the entrained-flow gasifier.

(9) Detailed SPIV measurements suggest that measured velocity profiles may be useful for simulation of counter-flow flames using axi-symmetric 2-D flame codes.

(10) Combined velocity and temperature measurements are necessary to fully understand the reacting flowfield in counter-flow flames.

5.0 Participating Personnel

This project represents a multidisciplinary collaboration between Chemical Engineers, Mechanical Engineers, and Aerospace Engineers benefitting from the knowledge base of all three disciplines. All personnel listed below are accessible to help on all parts of the project in addition to being focused on the three tasks as listed in the following.

Biomass Fast Hydropyrolysis: School of Chemical Engineering

1. Rakesh Agrawal, Professor, PI. Oversaw and participated in all aspects of the research related to biomass hydropyrolysis. Provides the overall vision for a sustainable transportation fuel economy.
2. Fabio H. Ribeiro, Professor, participating investigator. Participated in design and oversaw construction and operation of all equipment, participated in design and interpretation of all experiments.
3. W. Nicholas Delgass, Professor, participating investigator. Participated in design of equipment and design and interpretation of all experiments.
4. Andrew Smeltz, Lead Research Engineer. Oversaw and helped design and build and operate all experimental apparatuses, responsible for compiling research reports from group members.
5. Piotr Gawecki, Graduate Student. Helped design, build, and operate micro batch pyrolysis reactor used for visualization studies and compile data for reporting.
6. Vinod Kumar, Graduate Student. Helped design and build and operate all experimental apparatuses and compile data for reports.
7. Fernando Resende, Post-Doctoral Research Associate. Helped design, build, and operate prototype pyrolysis units.
8. Jun Wang, Post-Doctoral Research Associate. Helped design, build, and operate micro batch pyrolysis reactor used for visualization studies.
9. Yury Zvinevich, Director of the Advanced Spectroscopic Facility. Helped design and build visualization apparatuses used in the study.

Optically Accessible Gasifier and Flame Structure Studies: School of Mechanical Engineering and School of Aeronautical and Astronautical Engineering

1. Jay Gore, Professor, Co-PI. Oversaw and participated in all aspects of the research related to the optically accessible gasifier and flame structure studies. Provided overall coordination and support across the project.
2. Robert Lucht, Professor, participating investigator. Oversaw the design, construction and operation of counter flow burner experiment for flame structure studies. Provided expertise in design of experiment for optical diagnostics of gasifier.

3. Li Qiao, Assistant Professor, participating investigator, Oversaw the computational work related to flame structure studies. Provided her expertise related to coal gasifier modeling.
4. Scott Meyer, Operational director Maurice J. Zucrow Labs, Oversaw the design and construction of gasifier experimental apparatus and laboratory infrastructure.
5. Sameer V. Naik, Visiting Assistant Professor, Participated in design and operation of experiment for flame structure studies. Provided his expertise in design of experiment for optical diagnostics of gasifier. Performed HITRAN simulations of CO and H_2O.
6. Daniel R. Guildenbecher, Visiting Assistant Professor, Oversaw and participated in the design, construction, and experimental evaluation of the entrained-flow gasifier. Responsible for compiling research reports from group members.
7. Anup Sane, Graduate Student, Performed overall process calculations which established the research direction, led the design process of the high pressure particle feeder and optical diagnostics system.
8. David Blunck, Graduate Student, Oversaw and participated in the design process of gasifier rig, Worked as a project coordinator.
9. Rohan Gejji, Graduate Student, Led the design and manufacture of chemical steam generator and the assembly process of the optically accessible gasifier arrangement.
10. Indraneel Sircar, Graduate Student, Led the design of the reactor vessel, support structure, and control and diagnostics system for the gasifier arrangement.
11. Brent Rankin, Graudate Student, Performed infrared diagnostics of the H_2-O_2 chemical steam generator, assisted with the design and construction of the entrained-flow reactor.
12. Aman Satija, Graduate Student, Performed experimental work for flame structure studies.
13. Deepti Singh, Graduate Student, Computations of premixed and nonpremixed flames of surrogate and alternative fuels using CHEMKIN.
14. Saad Tanvir, Graduate Student, Computations of premixed and nonpremixed flames of surrogate and alternative fuels using CHEMKIN.

6.0 Publications and Presentations

6.1 Publications

1. Agrawal, R., Singh, N.R., "Solar Energy to Biofuels", An invited submission to Annual Review of Chemical and Biomolecular Engineering, 1, 343 (2010).
2. Singh, N.R., Delgass, W.N., Riberio, F.H., and Agrawal, R., "Estimation of Liquid Fuel Yields, Environmental Science and Technology, 44, 5298 (2010).
3. Singh, N.R., Mallapragada, D.S., Agrawal, R., Tyner, W.E., "Economic Analysis of Novel Synergistic Biofuel (H2Bioil) Processes", Submitted for publication to Biomass & Bioenergy.
4. Sircar, I., Gejji, R., Sane, A., Blunck, D., Mayer, S., and Gore, J., "Design and Testing of a High Pressure and High Temperature, Optically Accessible, Entrained Flow Coal Gasifier", ASME/JSME 8th Thermal Engineering Joint Conference, (2011), Honolulu, HI, March 13-17.
5. Sircar, I., Gejji, R., Sane, A., Blunck, D., Meyer, S., and Gore, J., "Design and Construction of an Optically-Accessible Coal Gasifier for CO_2 Reduction using Excess H_2", AIAA ASM Conference, (2011) Orlando, FL, January 4-7.
6. Gejji, R., Sane, A., Rankin, B., Sircar, I., Meyer, S., Gore, J. "An experimental study of superheated H2-O2 steam generator," 7th US National Combustion Meeting, (2011) Atlanta, GA, March 21-23.
7. Satija, A., Panda, P.P., Wagh, Y., Naik, S.V., Gore, J.P., Lucht, R.P. "Characterization of counter-flow methane-air and hydrogen-air flames using Stereo Particle Image Velocimetry (SPIV) and Coherent Anti-Stokes Raman Scattering (CARS)", 7th US National Combustion Meeting, (2011) Atlanta, GA, March 21-23.

6.2 Presentations

1. Agrawal, R., "Solar Based Sustainable Energy Solutions", Maddox Solar Energy Series, Whitacre College of Engineering at Texas Tech University, Lubbock, Tx, February, 2010.
2. Agrawal, R., "Solar Based Sustainable Energy Solutions", Plenary Lecture, 2nd International Symposium on Sustainable Chemical Product and Process Design (ISSCPPE), Hangzhou, China, May, 2010
3. Agrawal, R., "Transportation Fuel Solutions using Renewable Energy", EPFL, Lausanne, Switzerland. Sept 2010
4. Agrawal, R., "Chemical Engineering in a Solar Energy Driven Sustainable Future", PPG Foundation Keynote Address, 32nd Annual Chemical Engineering Graduate Student Association Symposium, Carnegie Mellon University, Pittsburgh, PA, October, 2010
5. Agrawal, R., "Solar Based Sustainable Energy Solutions", Pirkey Lecture, University of Texas, Austin, Tx, Nov. 2010
6. Agrawal, R., "Solar Based Sustainable Energy Solutions", Invited keynote address, AIChE annual meeting, Salt Lake City, UT, Nov 2010.